Renewable and Sustainable Energy Reviews 41 (2015) 413–435

Contents lists available at ScienceDirect

Renewable and Sustainable Energy Reviews

journal homepage: www.elsevier.com/locate/rser

Thermo-hydraulic performance analysis of solar air heaters having artificial roughness–A review

Sanjay K. Sharma*, Vilas R. Kalamkar

Department of Mechanical Engineering, Visvesvaraya National Institute of Technology, Nagpur 440010, India

ARTICLE INFO

Article history:
Received 29 March 2014
Received in revised form
5 August 2014
Accepted 16 August 2014

Keywords:
Artificial roughness
Thermo-hydraulic
Heat transfer
Solar air heater

ABSTRACT

Enhancement of heat transfer in the solar air heater ducts can be achieved by several means like using baffles, fins, ribs and groves. Until now, various attempts have been made to investigate the effects of these geometries on the enhancement of the heat transfer rate; however it is achieved at the cost of the increase in the pressure drop across the surfaces on which these elements are mounted. This paper is an attempt to summarize and conclude the investigations involving the use of small height elements and surface protrusions on absorber plate and channel walls as artificial roughness elements of various geometries and its effect on heat transfer and friction factor through experiments. It also summarizes the various correlations which have been developed for Nusselt number (Nu) and Friction factor (f) and reported in the previous investigations. The comparative study has been done to understand the results of these investigations for solar air heaters with different roughness elements on its absorber surface.

© 2014 Elsevier Ltd. All rights reserved.

Contents

* Corresponding author.
E-mail address: sksharma.cg@gmail.com (S.K. Sharma).

http://dx.doi.org/10.1016/j.rser.2014.08.051
1364-0321/© 2014 Elsevier Ltd. All rights reserved.

1. Introduction

The energy demand is growing continuously and rapidly, and it is impossible to meet the future demand with the presently available exhaustible energy sources. So, the technology is focusing on harnessing new and renewable sources of energy. Furthermore, the conventional energy sources are causing an alarming health hazard to the planet life. The use of solar energy is an intelligent option for the use of mankind which is available free of cost, in abundant and is a clean source for various applications [1]. The solar energy can be used directly or indirectly by converting it into thermal energy. Instead of direct use of solar energy, it is more useful when converted into thermal energy. Solar air heater is such a device, which converts solar energy into thermal energy. It can be used for various applications like the heating of building, wood seasoning, drying of crops of fruits and vegetables, chicken brooding [2] as well as curing of industrial products [3]. It has many advantages like low fabrication, installation, and operational costs, and can be constructed by using cheaper and lesser amount of material. However, its efficiency is poor. The lower efficiency of solar air heater is attributed to poor heat transfer characteristics of air, and also the air cannot be used as storage fluid due to low thermal capacity [4]. The low efficiency of the solar air heater can be increased either by increasing the surface area of the absorber plate or by using certain artificial geometries on the absorber plate with some adverse effect of the increase in frictional loss in ducts which is needed to be taken care of by using proper, geometrical parameters and flow conditions. The use of artificial roughness rib elements on the absorber plate is one of the effective ways which enhances the heat transfer coefficient of the air, thus increasing the heat transfer rate. These roughness rib elements breaks up the boundary layers and induces turbulence which results in heat transfer enhancement. These roughness elements being smaller in height as compared to duct size causes turbulence in the laminar sub layer adjacent to the wall without affecting the main turbulent zone in the flow. Several attempts have been made by various researchers in their experimental work to achieve the heat transfer enhancement through these solar air heaters by using different roughness elements on the surface of absorber plate. The researchers have used several geometries of artificial rib roughness elements with different parameters and materials till now. But still this area of research has large opportunity for doing novel work to achieve the heat transfer enhancement with new geometry with different parameters. This review is an attempt to summarize all these efforts and to arrive at a conclusion regarding the previous experimentation works and providing an opportunity in this area to the researchers to inquest the new materials, geometries and techniques to achieve the desired result of enhancement of heat transfer.

2. Fluid flow and heat transfer characteristics of roughened surface

Earlier experiments dealt with roughness elements in pipe flow with water as flowing liquid. Use of ribs in pipe flow was extensively studied by Nikuradse [5]. He developed the velocity and temperature profile for sand grain roughened pipe flow and contributed to the study of the laws governing turbulent flow of fluids in roughened tubes, channels, and along rough plane surfaces with the law of similarity given by his previous authors. Nikuradse defined three regions or range of the fluid flow based on roughness Reynolds number (e^+) through the roughened pipe which is described below.

(I) In the first range, the roughness height has no effect on the resistance for low Reynolds numbers. This range includes complete laminar flow and partly turbulent flow. The portion of turbulent flow included increases as the relative roughness height decrease.
For this region

$$0 < e^+ < 5$$
$$R(e^+) = 5.5 + 2.5 \ln(e^+) \quad (1)$$

(II) In the second region, called as transition range, the effect of the roughness height is higher. The resistance increases with the increase in Reynolds number. The resistance depends on the Reynolds number and relative roughness of the surface.
For this region

$$5 \le e^+ \le 70 \quad (2)$$

(III) The third region is the turbulent region where the resistance due to roughness is independent of the Reynolds number. It follows the quadratic law of resistance.
For this region

$$e^+ > 70 \quad (3)$$

The three regions are shown in Fig. 1.

Dipprey and Sabersky [6] studied on the application of a heat–momentum transfer analogy to flow over a rough surface. They investigated on closely packed sand grain type roughness in pipe flow with air as flowing fluid medium and assumed the roughness to be closely approximated to that used by Nikuradse in terms of Reynolds roughness number (e^+) for the sand grain roughness. Webb et al. [7] developed correlations to define the performance advantages of roughened tubes in the heat exchanger design compared to smooth tubes of equal diameter. They used repeated-ribs as the roughness element for their investigation. Firth and Mayer [8] investigated the heat transfer and the friction factor performance of four different types of artificially roughened surfaces with square transverse rib, helical rib, trapezoidal transverse ribs and three-dimensional surfaces in gas cooled reactor as shown in Fig. 2.

3. Heat transfer enhancement through artificial roughness

Artificial roughness and different obstruction used in the path of air passage in solar air heaters are used to increase the heat

Nomenclature

Physical parameters

A_b	absorber plate surface area, m^2
C_p	specific heat of air, J/kg K
W	width of duct
H	height/depth of duct
D_h	hydraulic diameter
e	roughness element height, m
P	Pitch, m
k	thermal conductivity of air, W/m K
h	heat transfer coefficient of air, W/m^2 K
m	mass flow rate of air, kg/s
ΔP	pressure drop, Pa
q_u	useful heat flux, W m^{-2}
Qu	useful heat gain, W
Q_L	heat loss from collector, W
Q_t	heat loss from top surface, W)
T_a	ambient temperature, K
T_i	fluid inlet temperature, K
T_o	fluid inlet temperature, K
T_{am}	mean air temperature, K
T_{pm}	mean plate temperature
w	width of rib, m
d	diameter of dimple or protrusion, m
L	length of test section of duct or longway length of mesh, m
G	mass flow rate of air, kg/s
I	Solar intensity, W m^{-2}
S	length of discrete rib or shortway length of mesh, m
g	groove position, m
W	width of duct, m
Re	Reynolds number
f	friction factor
e^+	roughness Reynolds number
F_P	plate efficiency
S/N	signal-to-noise ratio
Re_H	Reynolds number based on channel height

Geometric dimensionless parameters:

P/e	relative roughness pitch
e/D_h	relative roughness height
g/e	relative gap width
B/S	relative roughness length
l/s	relative length of metal grit
d/w	relative gap position
W/H	duct aspect ratio
W/w	relative width
g/p	relative groove position
G_d/L_v	relative gap distance
S/e	relative shortway length
d/D	relative print diameter
L/e	relative long way length of
e/d	height to print diameter of protrusion

Greek symbols

α	angle of attack, degree
Φ	rib chamfer/wedge angle, degree
ρ	density of air, m^3/kg
$\tau\alpha$	transmissivity–absorptivity product
η_{II}	exergy efficiency
β	collector slope
β^1	rib open area ratio

transfer rate either by breaking the laminar sub-layer or by increasing the turbulence in duct passage for air flow. Artificial roughness solves the first purpose and obstructions in the form of baffles, and winglets solve the second purpose. However, this increase in the thermal performance is gained at the cost of the increase in the pressure drop which requires pump or blower to supply energy to the fluid. The important phenomenon which helps to increase the heat transfer by using roughness elements in solar air heaters are (a) reattachment of flow, (b) formation of secondary flow, and (c) formation of vortices. These elements help in increasing the heat transfer performance characteristics of solar air heaters and also increase the friction loss. The maximum heat transfer occurs at the reattachment point which is due to the separation of flow and can be seen in the Figs. 3 and 4 [9]. The geometrical parameters of the roughness elements as well as the duct, such as rib to channel height ratio (e/D or e/D_h); pitch to the rib height ratio (P/e); duct aspect ratio, AR (W/H); angle of attack of rib (α); relative gap width (g/e); relative roughness length (B/S) etc. greatly affect the thermo-physical behaviour of the duct.

3.1. Parameters affecting the flow patterns

3.1.1. Rib height (e)

Ribs of certain height and alignment affect the flow by obstructing it and separating it from the main flow. Secondary flow can be seen along the ribs in the Fig. 5 and its mixing with the main flow. Vortices are also generated in the downside of flow behind the roughness element which causes turbulence, thus enhancing the heat transfer from the surface. For some types of ribs, the flow separation, free shears layer formation and vortices formation is shown in Fig. 6. In addition to that the frictional loss as well tends to occur due to vortices formation. The rib height is approximately 15% of the plate separation distance [10].

3.1.2. Rib pitch (P)

As the rib height and pitch changes there is a change in the flow pattern also which is clearly visible by Figs. 3 and 4. Due to the height, the flow in the downstream side of the roughness element is separated and if the pitch is not maintained properly reattachment of the flow does not occur. The reattachment of the shear layer does not occur for pitch ratio less than 8, and it will result in poor heat transfer from the surface. Maximum heat transfer occurs at the reattachment point. The local heat transfer coefficients in the separated flow region are larger than those of an undisturbed region [7]. When the relative roughness height ratio (e/D_h) is kept constant then also reattachment can be achieved by reducing the relative roughness pitch (P/e). As P/e increases from its lowest value, the friction factor and the heat transfer also increases. The maximum value of P/e occurs at about 10 [11].

3.1.3. Effect of rib alignment (p)

Rib alignment in the surface affects the performance of the solar air heater; the friction factor falls rapidly as the angle of attack decreases from 90° to 15° [11]. Secondary flow is generated along the rib surface which helps in increasing the heat transfer as

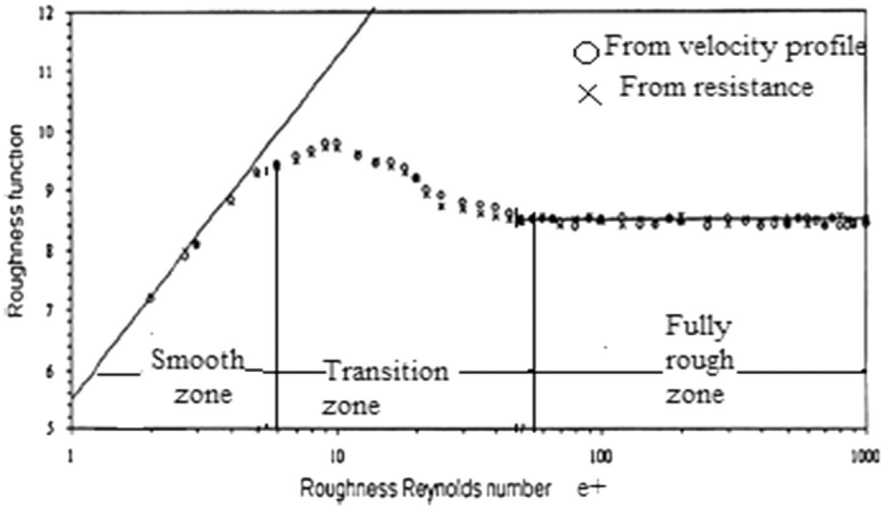

Fig. 1. Friction factor versus roughness Reynolds number.

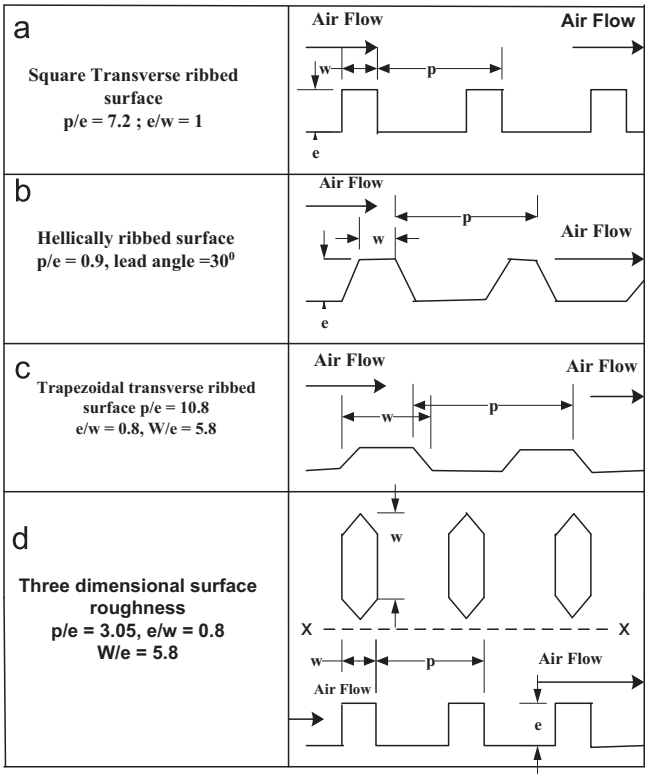

Fig. 2. Firth and Mayer's rib geometry.

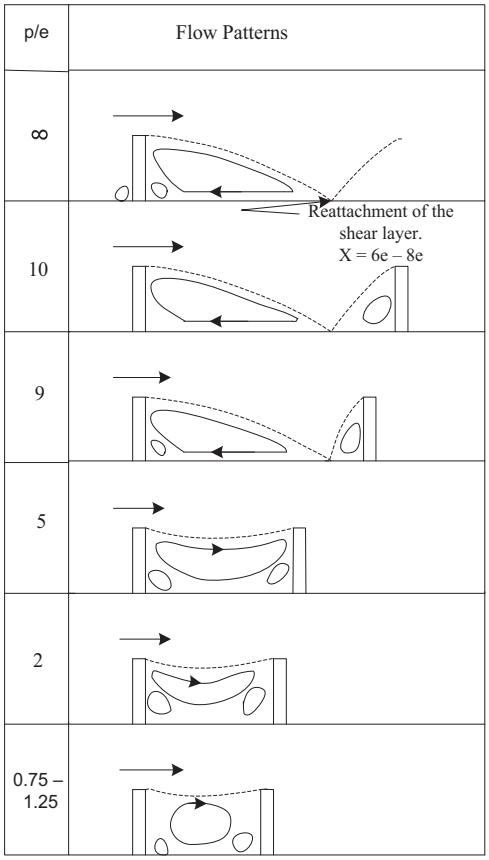

Fig. 3. Flow pattern downstream the roughness element as a function of roughness pitch ratio (*P*/*e*).

seen in Fig. 5. However, it also increases the friction factor. Fluid vortices are generated in the upstream and downstream side of rib. The two vortices meet the main stream at the tail end while moving along the rib surface [12]. These moving vortices mix up with the cold stream of air thus increasing the temperature of leading edge. The rib alignment has a very modest effect on the friction factor and the heat transfer [10].

3.2. Effect of geometrical dimensions on performance of solar air heater

3.2.1. Aspect ratio (W/H)

The aspect ratio has effect on the performance of solar air heaters. In large aspect ratio ducts friction is increased with increase in turbulence. The lower aspect ratio duct provides a better heat transfer performance [13]. For equal pumping power, the heat transfer performance of square channel is better than that of rectangular duct with aspect ratio 2 and 3 [14]. The collector efficiency increases with the increase in collector aspect ratio. As the aspect ratio increases, the cross sectional area of the air duct decreases and the velocity of flow increases so the convective heat transfer from the surface of the absorber plate to flowing air increases. In addition to enhancement in heat transfer it also increases the pumping power of the blower of pump leading to the increase in the operating cost of the equipment [15]. Increase in

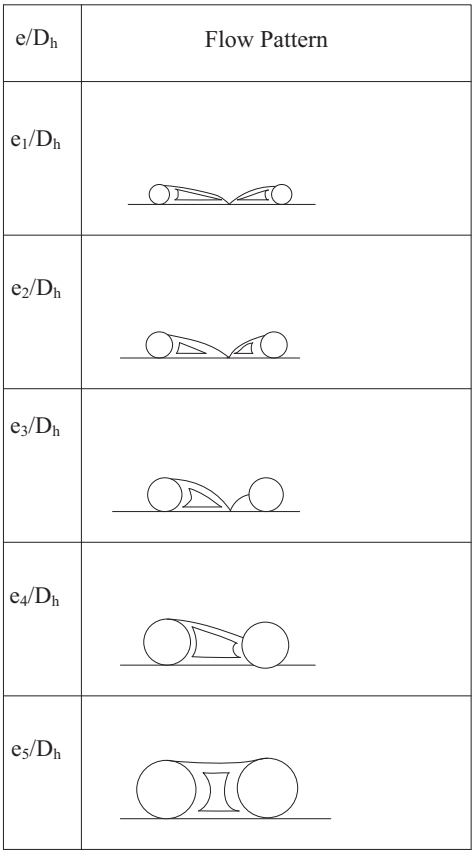

Fig. 4. Flow pattern for the roughness as a function of relative roughness height (e/D_h).

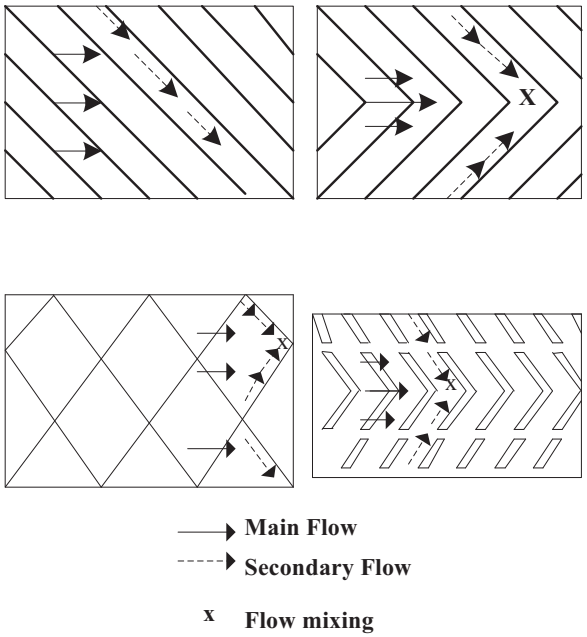

Fig. 5. Generation of secondary flow along different ribs.

heat transfer with increase in mass flow rate is also evident from the experiments with other type of heat exchangers like recuperators where when mass flow rate is increased there is net increase in the heat transfer to the flowing fluid [16].

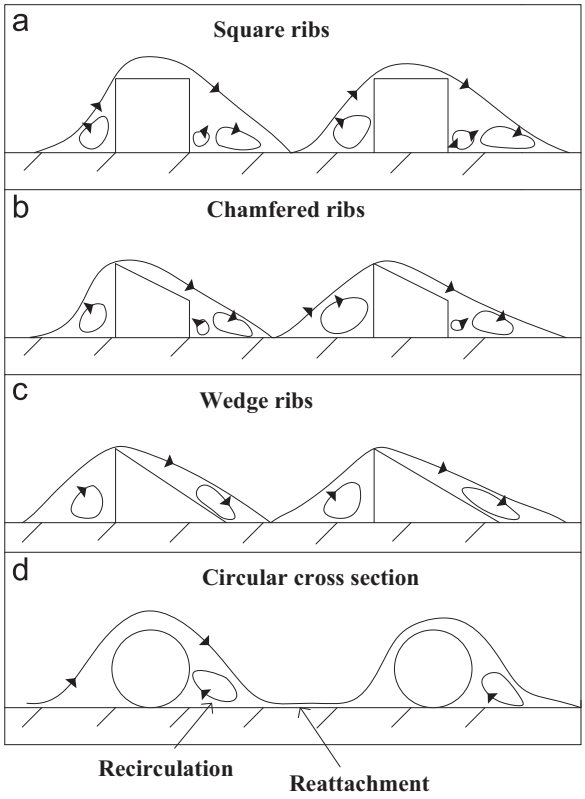

Fig. 6. Flow separation and vortices formation in different rib geometries.

3.2.2. Duct height (H)

Solar air heaters with lower duct height have higher efficiency. Lowering of duct height increases the air velocity. The effective efficiency decreases rapidly as the mass flow increases owing to the pumping power requirement which is proportional to ($1/H^3$) [11]. Solar air heater efficiency can be maximized by decreasing the depth of solar air heater along the length but in long channel along the length of the solar air heater causes substantial pressure drop causing high pumping losses [17]. An optimum mass flow rate corresponds to an optimum flow channel depth which is required to minimize annual cost to useful heat ratio [18]. At the optimum channel depth to length ratio the outlet temperature becomes equal to the absorber plate mean temperature [19].

3.2.3. Collector slope (β)

The collector slope affects the performance of the solar air heater. It is generally equal to the latitude of the place. However, 10–20° of higher value is recommended for winter season. A horizontal surface receives lower radiation in winter than the inclined surface [11].

4. Roughness elements used in channel flow

The initial efforts on using artificial roughness for improving heat transfer characteristics were confided with the areas of nuclear reactors, gas turbines blades, pipes carrying fluids and compact heat exchangers. Several types of artificial roughness elements were used extensively to improve the heat transfer characteristics in these equipments. The roughness elements of two dimensions, three dimensions and of irregular shapes were used by investigators like Nikuradse, Nunner and Dippery. Webb et al. [7] covers a wide range of e/D_h ratio with P/e values of more than 10 in his experiments in flow through pipes where the ribs

were aligned normal to the main stream direction. The experiments conducted with roughness in one wall, two walls and four walls of absorber plate. The roughness element in one wall is favoured by most of the investigators as discussed below in the range of Re=3000–30,000. Different correlations for heat transfer and friction factor were developed based on the experiments done by different investigators.

Bhargava and Rizzi [17] demonstrated that the efficiency of solar air heaters can be increased by decreasing the channel depth along the length. Hegazy [19] optimized the channel height of different types of the solar air heater. Han et al. [11] investigated the effects of rib shape, angle of attack and pitch to the height ratio on the friction factors and heat-transfer on symmetric and staggered ribs. They found that the ribs at 45° of attack angle have better performance than that at 90° attack angle and sand grain roughness. Han and Park [14] investigated the combined effects of the rib, angle-of-attack (α=90°, 60°,45° and 30°) and the channel aspect ratio (W/H=1, 2, 4) on the heat transfer coefficient in short rectangular channels (L/D=10 and 15) with two opposite rib-roughened walls. They concluded that the highest heat transfer, and the highest pressure drop can be obtained at α=60° in the square channel; the highest heat transfer and the pressure drop occur at α=90° with W/H=4 in the rectangular channel, and the values of highest heat transfer and pressure drop differs marginally at α=60° for W/H=2. They found that secondary flow or swirling flow moves along the rib surface producing higher Nusselt number towards the wall as compared to centre line. They also concluded that the highest heat transfer and highest pressure drop occur at α=90°. The heat transfer and friction correlations were also obtained for the surface. Hsieh et al. [20] investigated the effects of the aspect ratio (W/H)=1, 2, Reynolds number (Re) $63.5 < Re < 254$ and the initial boundary-layer thickness on low speed forced convective heat transfer near two-dimensional transverse ribs. They also derived the correlation for average Nusselt number. Hong et al. [21] investigated for turbulent flow on staggered ribs in a square duct with two opposite rib-roughened walls using the parameters of relative roughness height (e/D_H)=0.19; relative roughness pitch (P/e)=5.31 and Reynolds number (Re)=13,000–130,000. The temperature distribution and correlation between Nusselt number and Reynolds number was established. The heat transfer rate was calculated to be 2.02–4.60 times higher than the fully developed turbulent flow in smooth duct for Re=13.000. Hwang and Liou [22] investigated the thermo-hydraulic performance for a low aspect ratio channel with staggered slit ribs on top and bottom walls with the parameters of rib area open ratio (β^1)=24%, 37%, 46%; P/e=10, 15, 20; W/H=0.081; Re=10,000–50,000. They concluded that the arrangement of ribs gives a higher heat transfer enhancement with lower pressure drop for the same solid rib height and spacing. Also the friction factor decreases for an increase in rib open area ratio. They also developed the general friction and the heat transfer correlations have been developed. Gao and Sunden [23] investigated the heat transfer and pressure drop in a rectangular duct with staggered ribs of various parameters as the aspect ratio (W/H)=1–8; relative roughness height (e/D_H)=0.06; angle of attack (α)=60°; Reynolds number (Re)=1000–6000. They observed that secondary flow causes span wise variation of the heat transfer coefficients along the rib length, and reattachment occurs between two ribs. They concluded that the V downstream ribs induce the highest friction factor than V upstream and parallel ribs with least friction factor. V downstream has stronger secondary flow and gives higher heat transfer when compared to V upstream and parallel ribs also the parallel rib has better performance at higher Reynolds number than V upstream. Murata and Mochizuki [24] investigated on laminar and turbulent flow with transverse or angled rib turbulators of angle of attack of 60° or 90°

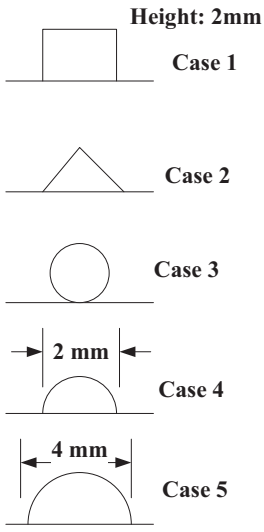

Fig. 7. Different geometries.

in a square channel. They concluded that heat transfer is highest in front of the rib, and laminar flow has the lesser effect on the flow field with ribs than turbulent flow as a result the velocity and temperature profiles have lesser differences than the turbulent case. Ahn [25] investigated on five different types of roughness element as shown in Fig. 7 in rectangular duct with e/D_H=0.0476, P/e=8, and W/H=2.33, to understand the comparative thermo-hydraulic performance due to these elements. He concluded that the triangular rib has the highest heat transfer capacity and Nusselt number is higher in the case of square and triangular ribs when compared to semicircular ribs. The square ribs have the highest friction factor.

Chandra et al. [26] investigated the effect with varying number of transverse ribbed walls with the parameters Re=10,000–80,000; P/e=8; e/D_H=0.0625 channel length to the hydraulic ratio (L/D_h)=20 for fully turbulent flow in the square channel. They concluded that one ribbed wall has the heat transfer increase of 2.43–1.78 for Re=12,000–75,000, with two opposite ribbed walls the increment was 2.64–1.92, with three ribbed walls, the increment of 2.81–2.01 and with four ribbed walls, an increment of 2.99–2.12 which is the maximum when compared to all the types. The maximum increase in the friction factor was found to be 9.50 with four sided ribbed walls and minimum with one ribbed wall of 3.14. They also compared the performance factor $\{(St_r/St_{ss})/(f_r/f_{ss})\}$ of four cases and concluded that, it is highest at 1.78–1.17 for one wall ribbed surface. Tanda [27] investigated for heat transfer coefficient distribution in the rectangular channel with transverse continuous, transverse broken and V-shaped broken ribs which is shown schematically in Fig. 8 with the parameters W/H=5; α=45° or 60°. Liquid crystal thermo-graphy was applied to the study of heat transfer from the ribbed surface. Tanda found the maximum performance of continuous transverse ribs of 45° V-shaped ribs and 60° V-shaped ribs at the optimum value of P/e=13.3, transverse broken ribs with P/e=4 and 8 give the higher heat transfer augmentation. Transverse broken ribs with P/e=4 and 13.3 give best thermal performance and transverse continuous ribs with P/e=4 and 8 give lesser heat transfer increment. Tariq et al. [28] investigated the heat transfer and flow characteristics in the entrance section of a rectangular channel with one and two solid ribs at the bottom surface. Tariq et al. used hot wire anemometry (HWA) and resistance thermometry (RTD) for measuring the velocity and temperature and Liquid crystal thermography (LCT) to trace temperature profiles, heat transfer coefficient evaluation and Nusselt number calculation. The various parameters used are $Re=2.09\times10^4$; P/e=10. They compared the results of experimentation and the theoretical energy balance and

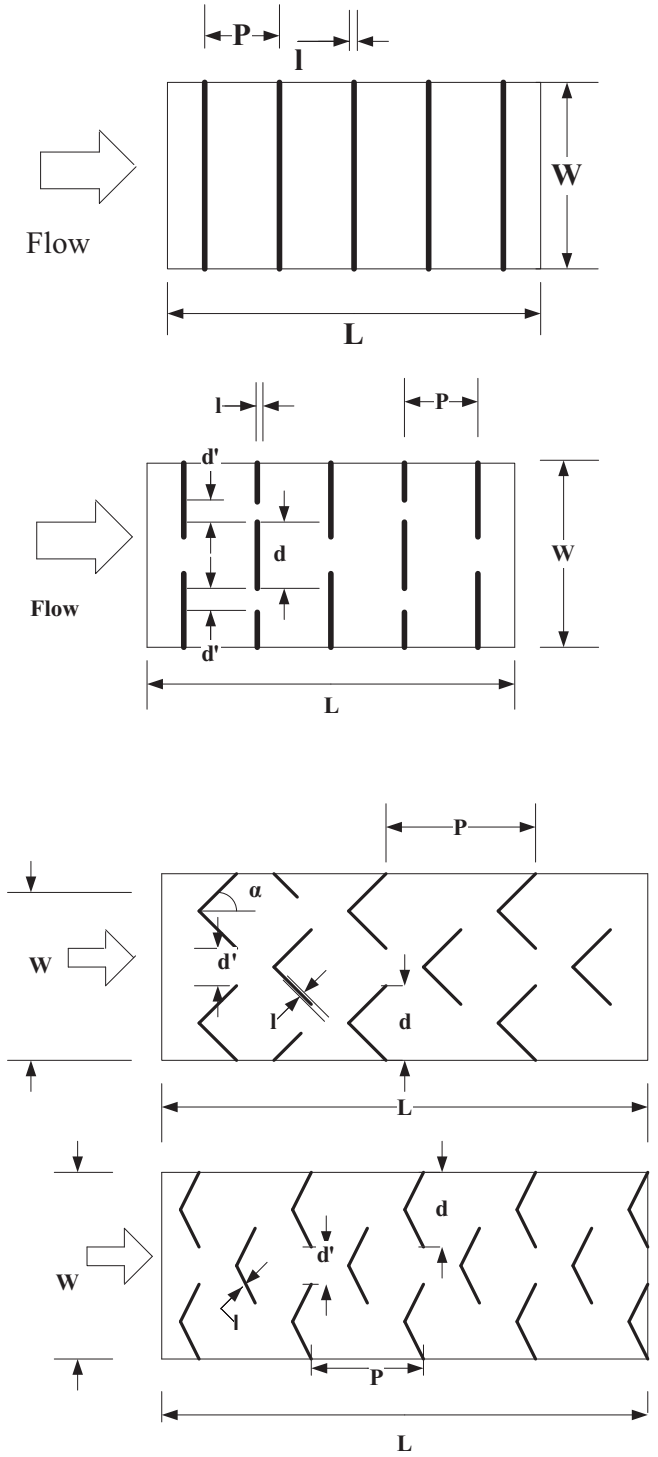

Fig. 8. Different rib geometries used by Tanda.

found similar performance under the given range of data selected. Won and Ligrani [29] compared the thermo-physical characteristics in channels with parallel and cross rib turbulators on two opposite surfaces with the parameters Reynolds number based on channel height (Re_H)=480–18,300; W/H=4; α=45°; e/D_H=0.078; P/e=10. Won and Ligrani found that the Nusselt number is almost same for the crossed and parallel-ribs, local Nusselt numbers for parallel-rib are significantly higher than crossed-rib and pressure loss is higher in central part of the channel. Wang and Sunden [30] performed an investigation of heat transfer and fluid flow in the rectangular channel with broken V-shaped up ribs using Crystal Thermography (LCT) and Particle Image Velocimetry (PIV) technique using the parameters e/D_h=0.06; P/e=10; α=60°; W/H=1/8. They concluded that the performance in heat transfer is higher than the continuous ribs bur with more friction loss.

5. Use of roughness elements in solar air heater

Liu et al. [31] investigated on heat transfer increment in a solar air heater with the absorber plate roughened by extended surfaces geometry. They found that the pressure drops rapidly when compared to heat transfer if the height of the roughened element is extended beyond the laminar sub layer. Prasad and Saini [9] investigated for the heat transfer rate and friction in fully developed turbulent flow in a solar air heater duct for the effect of height and pitch of the roughness elements of small diameter protrusion wires on the absorber plate. They also deduced expressions for the prediction of average Stanton number and friction factor. Prasad and Mullick [32] investigated on solar air heater with protruding wires in underside of the absorber plate. They found improvement of 9% (from 63% to 72%) in plate efficiency (F_P) for Reynolds number of 40,000. The plate efficiency is 44.5% higher in cross corrugated sheet with protruding wire than plane galvanized iron sheet. Gupta et al. [33] investigated the thermo-physical effect of transverse wire roughness on absorber plate on heat and fluid flow characteristics in transitionally rough flow region ($5 < e^+ < 70$) for rectangular solar air heater ducts with the parameters Reynolds number (Re)=3000–18,000 for a duct aspect ratio (W/H)=6.8–11.5, relative roughness height (e/D)=0.018–0.052 and relative roughness pitch (P/e)=10. They concluded that the heat transfer increased up to 1.8 times than that of smooth solar air heaters at α=60° and friction factor increases by 2.7 at α=70° for the range of parameters investigated. Saini and Saini [34] investigated for fully turbulent flow with expanded metal mesh as artificial roughness element. They used rectangular duct with W/H=11; relative long way length (L/e)=25–71.87; relative short way length (S/e)=15; e/D=0.012–0.039 as different parametric values for Re=1900–13,000. They concluded that the maximum values of Nusselt number and friction factor occurs at an angle of attack of 61.9° and 72°. Saini and Saini also developed the correlation for Nusselt number and friction factor. Gupta et al. [35] investigated on optimum design and operating conditions in artificially roughened solar air heater using the parameters e/D=0.023–0.05; Re=4000–18,000; solar intensity (I)=400–1300 W/m^2; α=60°. The optimum design conditions were determined and the correlation was developed for Reynolds number using the parameters selected for investigations. Ekkad and Han [36] investigated on two pass square channel solar air heater with rib tabulators with parameters Re=6000–60,000; e/D_H=0.125; P/e=10; α=90° parallel, 60° parallel, 60°V, and 60° broken V-shaped ribs. They investigated on thermo-physical characteristics and secondary flow before the 180° turn, in the turn region, after the turn, and the downstream in the second pass through the channel. They concluded that Nusselt number ratios in the second pass are 2–3 times higher than that for the first pass and the 60° parallel. Also 60° broken V ribs give the high-heat transfer rate in the first pass and 60° broken V ribs gives slightly better heat transfer, while, 60° parallel ribs give higher heat transfer in the turn and second pass respectively.

Verma and Prasad [37] investigated for optimal performance parameters in the form of Reynolds roughness numbers (e^+) and thermal efficiency ($\eta_{thermal}$) for the artificially roughened solar air heaters using the parameters Re=5000–20,000; mass flow rate ($\dot{m}$)=0.01–0.06 kg/s; P/e=10–40; e/D=0.01–0.03 and e^+=8–42. They found out the optimal value of e^+ optimum=24 at which $\eta_{thermal}$=71%, thus significant increase in heat transfer is achieved

using artificial roughness in solar air heaters. Singh et al. [38] investigated the heat and fluid flow characteristics of the solar air heater with discrete V down ribs as roughness elements with the parameters Re=3000–15,000; relative gap width (g/e)=0.5 to 2; relative gap position (d/w)=0.20–0.80; P/e=4–8; α=30–75° and e/D_h=0.015–0.043. They also developed the correlations for Nusselt number and friction factor for the given range of parameters selected. The maximum increase in Nusselt number and friction factor obtained are 3.04 and 3.11 at the optimum values of parameters of d/W=0.65, g/e=1.0, P/e=8.0, α=60° and e/D_h=0.043. Momin et al. [39] investigated the effect of V-shaped ribs as roughness elements in the underside of the absorber plate of the solar air heater with geometrical parameters as Re=2500–18,000; e/D_H=0.02–0.034; α=30–90°; P/e=10; W/H=10.15. They found the increase in heat transfer and friction of 2.30 and 2.83 more than that of smooth duct at α=60°, also in comparison to inclined ribs the enhancement in heat transfer was 1.14. They also developed the correlation for Nusselt number and friction factor for the V-shaped ribs. Karwa [40] investigated the thermo-physical behaviour of the roughened solar air heater with transverse, inclined, V continuous and V discrete ribs, as shown in the Fig. 8 with α=60° for inclined and V patterns for the parameters Re=2800–15,000; R (e^+)=17–90. Karwa also developed heat transfer and friction factor correlation based on the law of wall similarity and heat momentum transfer analogy. He found the increase in heat transfer of 65–90%, 87–112%, 102–137%, 110–147%, 93–134%, and 102–142% respectively whereas the increase in friction factor for the ribs were 2.68–2.94, 3.02–3.42, 3.40–3.92, 3.32–3.65, and 2.35–2.47, respectively (Fig. 9).

Sahu and Bhagoria [41] investigated the heat transfer coefficient in the solar air heater using 90° broken integral transverse ribs on an absorber plate with the parameters W/H=8; Re=3000–12,000; P/e=6.67, 13.33, 20; e/D_H=0.0338 and I=750–880 W/m^2. They concluded that maximum heat transfer and efficiency of 83.5% occurs at P/e=1.33.

Jaurker et al. [42] investigated the thermo-physical characteristics of combination of rib and groove geometry as artificial roughness in rectangular solar air heater duct with the parameters Re=3000–21,000; e/D=0.0181–0.0363; P/e=4.5–10; relative groove position (g/p)=0.3–0.7. Jaurker et al. also developed the correlations for Nusselt number and friction factor. They concluded that rib-grooved duct with P/e=6.0 and g/p=0.4 gives the maximum value of the Nusselt number of 2.75 and with P/e=6.0, g/p=0.4, and e/D=0.0363, the maximum value of the friction factor is 3.61. Mittal et al. [43] investigated the effect of various types of the roughness elements on the absorber plate of the solar air heater with the parameters W/H=10; e/D=0.02–0.04; P/e=10; Re=2000–24,000 to find out the effective efficiency using the correlations for heat transfer and friction factor developed by various investigators for the range of parameters they used. They concluded that the inclined ribs with low values e/D has high effective efficiency for Re > 12,000, expanded metal mesh has better effective efficiency for Re < 12,000 and effective efficiency of smooth solar air heater is higher than the solar air heaters with roughness for very high Reynolds number. Karmare and Tikekar [44] investigated the effect of the solar air heater roughened with metal grit ribs with parameters e/D_h=0.035–0.044; P/e=12.5–36; relative length of grit (l/s)=1.72–1 and Re=4000–17,000. They also developed correlation for Nusselt number and friction factor within the range of parameters selected. They concluded that within the range of parameters, at l/s=1.72, e/D_h=0.044, and P/e=17.5 gives the optimum performance.

Aharwal et al. [45] investigated the thermo-hydraulic performance of the solar air heater with inclined continuous rib with a gap with the parameters W/H=5.84; P/e=10; e/D_h=0.0377; α=60°; g/e=0.5 to 2; d/W=0.1667–0.667; Re=3000–118, 000. They found the maximum increase in Nusselt number and friction factor to be 2.59 and 2.87 at the optimum values of parameters at g/e=0.5 and d/W=0.25 for the range of parameters selected. Saini and Verma [46] investigated the effect of dimple shaped artificial roughness for solar air heaters with the parameters as Re=2000–112,000; e/D=0.018–0.037; P/e=8–112. Furthermore, correlation was developed for Nusselt number and friction factor for the given range of parameters. They found that maximum Nusselt number occurs at P/e=10 and e/D=0.0379 and minimum friction factor at P/e=10 and e/D=0.032. Saini and Saini [47] conducted an experimental study with arc shaped parallel wire as the roughness element in solar air heater with the parameters W/H=12;

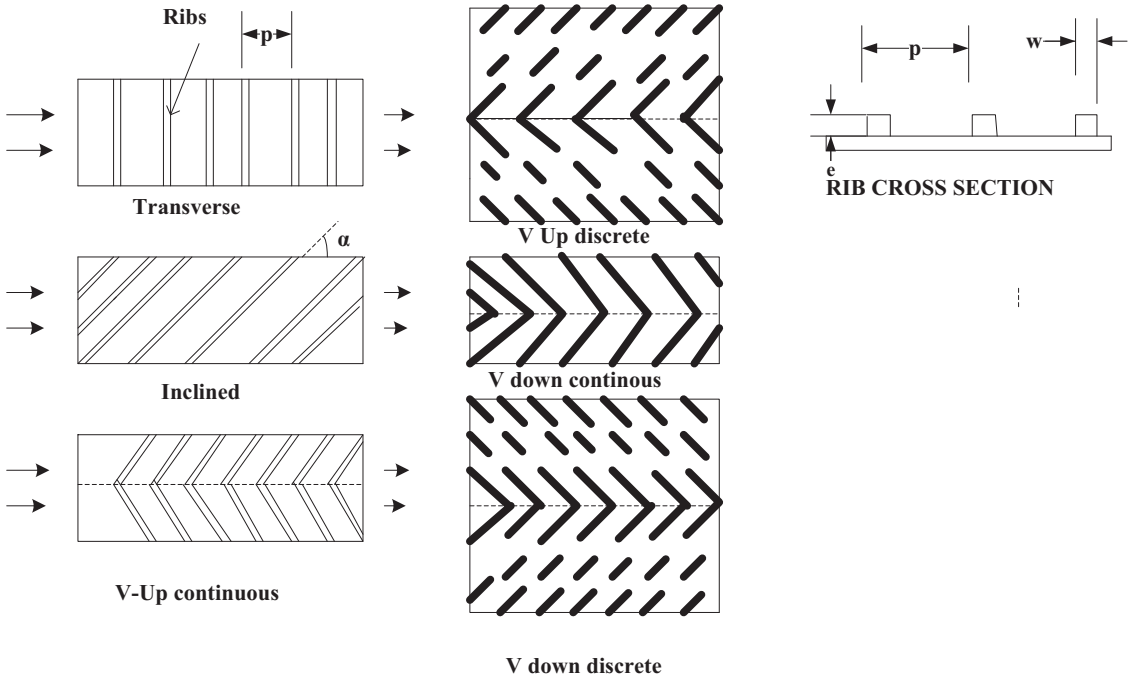

Fig. 9. Different rib geometries used by Karwa.

e/D=0.0213–0.0422; Re=2000–117, 000; P/e=12; $\alpha/90$=0.333–0.0.666. They also derived the correlations for Nusselt number and friction factor for the range of parameters selected. They concluded that at $\alpha/90$=0.3333, the maximum heat transfer coefficient obtained is 3.80 and the friction factor is maximum for the highest value of $\alpha/90$ of 1.75 in comparison to smooth solar air heater duct.

Layek et al. [48] studied the effect of chamfering of compound turbulators of rib and groove on the absorber plate in solar air heater with the parameters P/e=10; e/D_h=0.03; g/P=0.5; Re=3000–21,000; 600 V groove; Φ=5°,12°,15°,18° and 30°. They concluded that the Nusselt number is maximum of 2.6 at Φ=18° and increase in friction factor is 3.35 for the same angle. Furthermore, the thermo-hydraulic parameter (η)=Nu/Nu$_s$ is 1.4 and 1.76 for the range of parameters considered as compared to the smooth solar air heater. Kumar et al. [49] investigated the thermo-physical performance of solar air heaters with discretized W-shaped roughness elements on the absorber plate with the parameters W/H=8; e/D_h=0.0168–0.0338; P/e=10; α=30–75°; Re=3000–15,000. Kumar et al. also developed the correlations for Nusselt number and friction factor using the range of parameters selected. They found that the increase in Nusselt is 2.16 and friction factor is 2.75 at e/D_h=0.0338 and α=60° as compared to smooth solar air heater. Aharwal et al. [50] investigated the solar air heater with integral inclined discrete ribs on the absorber plate with parameters W/H=5.83; d/W=0.16–0.5; g/e=0.5–2.0; P/e=4–10; e/D=0.018–0.037; α=30–90°; Re=3000–18,000. Aharwal et al. also developed the correlations for the Nusselt number and friction factor for the given range of parameters selected. They found the increase in Nusselt number of 2.83 and friction factor of 3.60 as compared to smooth solar air heaters at the optimum values g/e=1, d/w=0.25, P/e=8, α=60°, e/D=0.037 of the parameters. Gupta and Kaushik [51] investigated the effect on energy augmentation ratio (EAR), effective energy augmentation ratio (EEAR) and exergy augmentation (EXAR) with expanded metal mesh as the roughness element on the absorber plate of the solar air heater. They concluded that all the three parameters increases with the increase in duct depth and solar intensity. The EAR is high for the parameters investigated. However, pump work requirement also increases and higher EXAR is obtained for high duct depth and low Reynolds number.

Karmare and Tikekar [52] investigated on the thermal energy (η_{th}) increment of solar air heater using artificial roughness with the parameters e/D_h=0.035–0.044; P/e=15–17.5; l/s=1.72, and Re=3600–17,000. They concluded that the increase in thermal η_{th} is 10–35% and the friction factor is 80–250%. They also developed the relation for parameters yielding optimum performance. Bopche and Tandale [53] investigated the thermo-hydraulic characteristics of inverted U-shaped turbulator roughened solar air heater with the parameters Re=3800–18,000; e/D_h=0.0186–0.03986; P/e=6.67–57.14; α=90°. They also developed the correlations for the Nusselt number and friction factor for the range of parameters selected. They concluded that the increase in Nusselt number and friction factor is 2.82 and 3.72 times higher than the smooth solar air heater for the range of parameters selected. Varun et al. [54] investigated the effect on effective efficiency (η_{eff}) of transverse and inclined ribs as artificial roughness on the absorber plate of the solar air heater with the parameters Re=2000–14,000; P/e=3–8; e/D=0.030. They optimized η_{eff} for the range of parameters selected using the Taguchi method. Varun et al. concluded that the signal-to-noise (S/N) ratio of the heat transfer coefficient and η_{th} is found to be 13.42 db and −9.41 db and the maximum η_{eff} occurs at P/e=8 for the range of parameters considered.

Karwa and Chauhan [10] investigated the performance of the solar air heater in terms of thermal (η_{th}) and effective (η_{eff}) efficiencies using V-down discrete ribs on at the absorber plate with the parameters β=0° and 90°;W/H=200; e^+=15–75; Re=1070–26,350; e/D_h=0.02–0.07, and I=0.037 Wm^{-1} K^{-1}; $\dot{m}$=0.01–0.06 kg s^{-1} m^{-1}; and α=6600. They concluded that the η_{th} is higher below 0.04 kg s^{-1} m^{-2} and differs slightly with η_{eff}, however, at higher $\dot{m}$, η_{th} is higher than η_{eff}. Hans et al. [55] investigated the solar air heater with multiple V-shaped ribs on absorber with the parameters=2000–20,000, e/D=0.019–0.043, P/e=6–12, α=30–75°, W/w=1–10. They developed the correlations for the Nusselt number and friction factor for the range of parameters selected. They found that the Nusselt number at W/w=6 and friction factor at W/w=10 increased by 6 and 5 at P/e=8 higher than smooth solar air heaters.

Lanjewar et al. [56] investigated on the effect of W-shaped rib roughness in solar air heater duct with the parameters W/H=8.0; P/e=10; e/D_h=0.018– 0.03375; α=30–75°, and Re=2300–14,000. Lanjewar et al. developed the correlations for the heat transfer coefficient and friction factor for the given range of parameters selected. They concluded that the maximum increase in Nusselt number is 2.36 with friction factor of 2.01 at α=60° and maximum enhancement in thermo-hydraulic performance $\{(Nu_r/Nu_s)/(f_r/f_s)\}^{1/3}$ is maximum at e/D_h=0.03375 and α=60°, and it is better than the V-shaped ribs. Tanda [57] investigated the effect of angled continuous ribs (P/e=6.66, 10, 13.33, 20; α=45°;), transverse continuous (P/e=13.33; α=90°), transverse broken ribs (P/e=13.33; α=90°), and discrete V-shaped ribs (α=45°, 90°; P/e=13.33) on the absorber plate on heat transfer enhancement with the other parameters e/D=0.09; e/H=0.15, and Re=9000–40,000 being constant for all the types of ribs. Tanda concluded that the highest heat transfer and the friction factor is given by transverse broken and the transverse continuous ribs and the transverse broken ribs have best relative heat transfer performance when the pumping power is kept constant. Lanjewar et al. [58] investigated the thermo-hydraulic effect of different W-up shape and W-down shape of W rib roughness in solar air heater with the parameters of W/H=8.0, P/e=10; e/D_h=0.03375; α=30–75°; Re=2300–14,000. They also developed the heat transfer and friction factor correlations in the range of parameters selected. They concluded that W-down shaped rib gives the best thermo-hydraulic performance $\{(Nu_r/Nu_s)/(f_r/f_s)\}^{1/3}$=1.98 at α=60°, e/D_h=0.03375 and P/e=10.

Kumar et al. [59] performed investigations of the solar air heater with multi V shape with a gap as rib geometry to find out the thermo-physical characteristics with the parameters Re=2000–20,000, W/w=6, G_d/L_v=0.24–0.80, g/e=0.5–1.5; e/D=0.043, P/e=10; α=60°. They found out the maximum increase in Nusselt number and friction factor to be 6.32 and 6.12 at the optimum parameters g/e=1 and G_d/L_v=0.69. Bhusan and Singh [60] investigated the effect of protruded absorber plate on the thermal and hydraulic characteristics with S/e=18.75–37.5; l/e=25.0–37.5; d/D=0.147–0.367 as variable parameters and find out the optimum values of these parameters for η_{th} and η_{eff} of the absorber plate. They found the values of η_{th} and η_{eff} to be 2.3 and 2.2 as compared to the solar air heater with smooth absorber plate. Bhushan and Singh [61] investigated the solar air heater with protrusion on at the absorber plate as the roughness element with the parameters S/e=18.75–37.50; L/e=25.00–37.50; d/D=0.0.147–0.367; e/D=0.03; W/H=10 and Re=4000–220,000. They also developed the correlation for Nusselt number and friction factor in the range of parameters selected. They concluded that the maximum value of Nusselt number occurs as 3.8 and friction factor of 2.2 for the parameters S/e=31.25, L/e=31.25 and d/D=0.294. Sethi et al. [62] investigated the solar air heater with dimple shape roughness element on at the absorber plate with the parameters W/H=11; P/e=10–20; e/D_h=0.021–0.036; α=45–75° and Re=3600–18,000. They also found the correlation for Nu and f for

the given range of parameters. They found the increase of Nusselt number and friction factor at the $P/e=10$; $e/D_h=0.036$, and $\alpha=45^\circ$. Singh et al. [63] investigated the thermo-hydraulic performance due to flow attack angle in V down rib in solar air heater with the parameters $W/H=12$; $Re=3000–115,000$; $e/D_h=0.043$; $\alpha=30–75^\circ$. They concluded that the thermo-hydraulic performance based on pumping power (η)=2.06, the Nusselt number and friction factor are highest for $\alpha=60^\circ$.

Kumar et al. [64] investigated solar air heater with multi V shape with gap rib on the absorber plate with the parameters Re=2000 to 20, 000; relative gap distance (G_d/L_v)=0.24–0.80; relative gap width (g/e)=0.5–1.5; $e/D=0.022–0.043$; $P/e=6–12$;

Table 1
Authors, roughness elements and various parameters.

Sr. no.	Authors	Roughness element	Reynolds no.	Non dimensional geometric parameters and values			
				P/e	e/D_h	α	Others
1	Prasad and Saini [9]	Transverse ribs	5000	10–20	0.020–0.033		
2	Saini and Saini [34]	Expanded metal mesh	1900–13,000		0.012–0.0390		$W/H=11$, $L/e=25–71.87$, $S/e=15$
3	Gupta et al. [35]	Small diameter traverse rib	4000–18,000	10	0.02–0.05	60°	
4	Mulluwork et al. [68]	V-Shaped staggered discrete wire ribs			0.02	60°	$B/S=3–9$
5	Karwa et al. [69]	Machined Ribs	3000–20,000	4.5–8.5	0.014–0.0320		$d/w=0.167–0.5$, $W/H=5.87$
6	Verma and Prasad [37]	Small diameter transverse protrusion wire	5000–20,000	10–40	0.01–0.03		
7	Momin et al.[39]	V-shaped continuous wire rib	2500–18,000	10	0.02–0.034	30–90°	
8	Bhagoria et al.[70]	Wedge shaped ribs	3000–18000	$60.17\Phi^{-1.0264} < P/e$ 12.12	0.015–0.033		$\Phi=8–15^\circ$
9	Karwa et al. [40]	Transverse, inclined, V shaped inclined and continuous	2800–15000			60°	
10	Sahu and Bhagoria [41]	Broken integral transverse ribs	3000–12,000	6.67–20	0.0338		$W/H=8$
11	Jaurker et al.[42]	Rib and groove combination		4.5–10	0.018–0.0363		$g/p=0.3–0.7$
12	Karmare and Tikekar [44]	Wire ribs-grid shape	3600–17,000	12.5–36	0.035–0.044	60°	$l/s=1.72–1$
13	Aharwal et el. [45]	Inclined continuous with gap ribs	3000–21,000	10	0.0377	60°	$d/w=0.167–0.5$, $W/H=5.87$, $g/e=0.5$, $d/w=0.167–0.5$
14	Varun et al.[54]	Inclined and transverse wire ribs	2000–14,000	10	0.030		
15	Saini and Saini [47]	Arc shaped wire ribs	2000–12000	12	0.0213–0.0422	30°–60°	$W/H=5.87$, $g/e=0.5–2$
16	Saini and Verma. [46]	Dimple protrusions	2000–17,000	8–12	0.018–0.037		
17	Varun et al.[72]	Inclined and transverse combination	2000–14,000	3–8	0.030		
18	Layek et al. [48]	Chamfered compound rib	3000–21000	10	0.03	5–30°	$g/p=0.5$
19	Karmare et al. [52]	Metal grit rib	40,000–17,000	15–17.5	0.035–0.044		$l/s=1.72$
20.	Kumar et al. [49]	Discritized W shape rib	3000–15,000	10	0.0168–0.0338	30–75°	$W/H=8$
21.	Aharwal et al. [50]	Integral inclined discrete rib	3000–18,000	4–10	0.018–0.037	30–90°	$g/e=0.5–2$, $d/W=0.16–0.5$
22.	Bopche and Tandale [53]	U shaped rib	3800–18,000	6.67–57.14	0.0186–0.03986	90°	
23.	Hans et al. [55]	Multiple V shape rib	2000–20000	6–12	0.019–0.043	30–75°	$W/w=1–10$
24.	Lanjewar et al. [56]	W shaped rib	2300–14,000	10	0.018–0.03375	30–75°	$W/H=8.0$
25.	Singh et al. [73]	Discrete V shape ribs	3000–15,000	4–8	0.015–0.043	30–75°	$g/e=0.5–2$, $d/w=0.20–0.80$
26.	Lanjewar et al. [58]	W shape with different orientations	2300–14,000	10	0.03375	30–75°	$W/H=8$
27.	Bhusan and Singh [61]	Protrusion	6000–62,000		0.03		$L/e=25–37.5$, $S/e=18.75–37.5$, $d/D=0.147–0.367$, $W/H=10$
28.	Sethi et al. [62]	Dimple shape in arc shape	3600–18,000	10–12	0.021–0.036		
29.	Kumar et al. [59]	Multi V shape with gap rib	2000–20,000	10	0.043	60°	$g/e=0.5–1.5$, $e/D=0.022–0.043$, $W/w=6$, $G_d/L_v=0.24–0.80$
30.	Kumar et al. [64]	Multi V shape with gap rib	2000–20,000	6–12	0.022–0.043	30–75°	$g/e=$ 0.5–1.5 $e/D=0.022–0.043$, $W/w=1–10$, $G_d/L_v=0.24–0.80$
31.	Yadav et al. [67]	Circular protrusion in arc shape	3600–18,100	12–24	0.015–0.03	45–75°	$W/H=11$, $e/d=0.3$

relative roughness width ratio (W/w)=1–10, α=30–75°. They also developed the correlations for Nusselt number and friction factor for the range of parameters selected. They concluded that the maximum increase in the Nu and f is found to be 6.74 and 6.37 at G_d/L_v=0.69; g/e=1; e/D=0.043; P/e=8; W/w=6 and α=60°. Prasad [65] investigated the thermal performance of solar air heater using thin G.I. wires of varying diameter for collector heat removal factor (F_R), collector efficiency factor (F') and thermal efficiency (η_{th}) under actual outdoor conditions using the parameters Re=2959–12631; m=0.0063 and 0.0259; P/e=10–40; e/D=0.0092–0.0279. Prasad concluded that the values of F_R, F' and η_{th} are increased by 1.786, 1.806 and 1.842 in comparison to smooth solar air heater. Karwa and Chitoshiya [66] investigated the performance of solar the solar heater with 600 V down discrete ribs on absorber plate and developed the mathematical relation using the various parameters of the rib for the heat transfer. Yadav et al. [67] investigated on the thermo-hydraulic characteristics of solar air heater having the protrusion on the absorber plate as roughness the roughness with the parameters W/H=11; Re=3600–18,100; P/e=12–24; e/D=0.015–0.03 and α=45° to 75°. They developed the correlations for Nusselt number and friction factor for the range of parameters selected. The found out the increment in heat transfer and friction factor were 2.89 and 2.93 times as compared to smooth solar air heater.

6. Different rib geometries used and their effects in solar air heater

Ribs of different geometries and orientation are extensively used for heat transfer enhancement in solar air heater. The ribs of circular and square shapes are used either in discritized form or continuous. The various rib geometries used by researchers and its effect on fluid flow, heat transfer and pressure drop are discussed below. The various types of rib geometries investigated are given in Table 1.

For each investigation of different authors, the optimum values of the parameters have been found out for the maximum increase in heat transfer. The optimum values of the different parameters have been given in Table 2 for the range of parameters selected.

6.1. Transversed ribs

Sahu and Bhagoria [41] investigated the solar air heater with 90° broken ribs on absorber plate surface and found the increase in the heat transfer coefficient of 1.25–1.4 times higher than smooth solar heaters. The rib arrangement is shown in Fig. 8. The heat transfer enhancement is due to flow separation due to rib and reattachment of flow in between the ribs. The ribs also help in formation of recirculation zones in the upstream side of the flow.

6.2. Inclined ribs

Gupta et al. [35] investigated on 60° inclined ribs at P/e=10 as shown in the Fig. 10 and concluded that at P/e=0.023 the roughened surface solar air heater is more thermodynamically efficient for the range of parameters investigated. Aharwal et al. [45] investigated on inclined rib with a gap of various parameters ranging from relative gap position (d/W)=0.167–0.5 and relative gap width (g/e)=0.5–2 as shown in the Fig. 11. They found enhancement in Nusselt number and friction factor to be 2.59 and 2.87 when compared to smooth solar air heaters. The gap in the inclined ribs helps the mixing up of secondary flow and main flow thus accelerating it and increasing the heat transfer through the gap width area behind the ribs.

6.3. V shaped ribs

Mulluwork et al. [68] investigated with comparative study of discrete V up and down ribs with transverse discrete staggered ribs as shown in Fig. 12. They concluded that the thermodynamic performance of V down discrete ribs is better than V up and

Table 2
Authors, roughness elements and optimum values of parameters obtained.

S. no.	Authors	Roughness Element	Reynolds no. (Re)	Optimum performance parameter values of roughness elements			
				P/e	e/D_h or e/D	α	Others
1.	Prasad and Saini [9]	Transverse ribs	5000	10	0.027		
2.	Saini and Saini [34]	Expanded metal mesh	1900–13,000		0.037	60°	L/e=46.87; S/e=25; W/H=11
3.	Gupta et al. [35]	Small diameter traverse rib	4000–18,000	10	0.033	61.9°	
6.	Karwa et al. [69]	Chamfered ribs	3000–20,000	5.5	0.0143		W/H=7.75; Φ=15°
7.	Verma and Prasad [37]	Small diameter transverse protrusion wire	5000–20,000	20	0.0145		e^+opt=24
8.	Momin et al. [39]	V-shaped continuous wire rib	17,034	10	0.034	60°	
9.	Bhagoria et al. [70]	Wedge shaped ribs	3000–18,000	7.57	0.033		Φ=10°
11.	Sahu and Bhagoria [41]	90° broken transverse ribs	3000–12,000	13.333	0.0338		
12.	Jaurker et al.[42]	Rib and Groove Combination	3000–21,000	6	0.0363		g/p=0.4
13.	Karmare and Tikekar [44]	Metal grit ribs	40,000–17,000	17.5	0.044		l/s=17.5
14.	Aharwal at el. [45]	Inclined continuous with gap ribs	3000–21,000	10	0.0377	60°	W/H=5.84; g/e=1; d/W=0.25
16.	Saini and Saini [47]	Arc shaped wire ribs	2000–17,000	10	0.0422		$\alpha/90$=0.3333
17.	Saini and Verma [46]	Dimple protrusions	2000–12,000	10	0.0379		
18.	Varun et al.[72]	Inclined and transverse combination	2000–14,000	8	0.030		
19.	Layek et al. [48]	Chamfered rib and groove	3000–21,000	10	0.03		Φ=18°
20.	Kumar et al. [49]	Discritized W shape rib	3000–15,000	10	0.0338	60°	
21.	Aharwal et al. [45]	Integral inclined discrete rib	3000–18,000	8	0.037	60°	d/W=0.25; g/e=1
22.	Bopche and Tandale [53]	U shaped rib	3800–18,000	6.67	0.03986	90°	
23.	Hans et al. [55]	Multiple V shape rib	2000–20,000	8	0.03	60°	W/w=10
24.	Lanjewar et al. [56]	W shaped rib	2300–14,000	10	0.03375	60°	W/H=8
25.	Singh et al. [73]	Discrete V down ribs	3000–15,000	8	0.043	60°	d/w=0.65; g/e=1
26.	Lanjewar et al. [56]	W shape with different orientations	2300–14,000	10	0.03375	60°	W/H=8
	Singh et al. [63]	V down ribs with gap	3000–15,000	8	0.043	60°	W/H=12
27.	Bhusan and Singh [61]	Protrusion	6000–62,000				S/e=31.25; L/e=31.25; 0.294
28.	Kumar et al. [64]	Multi V shape with gap rib	2000–20,000	10	0.043	60°	g/e=1; G_d/L_v=0.69; W/w=6
30.	Yadav et al.[67]	Circular protrusion	3600–18,100	12	0.03	60°	
31.	Prasad [65]	GI wires of varying diameter	2959–12,631	10	0.0279		G=0.0171

discrete staggered ribs with the enhancement in Stanton number found to be 1.37–2.47, also the friction factor was maximum for V down discrete ribs. Momin at al. [39] investigated the thermo-physical effects due to V shape roughness element of 300 and 90°. The maximum enhancement in Nusselt number was found to be 2.83 for $P/e=0.034$ and $\alpha=60°$. The flow separation in the secondary flow and the movement of the vortices causes the maximum heat transfer. The thermal and hydraulic performance $\{(St_r/St_s)/(f_r/f_s)\}^{1/3}$ as given by Webb and Eckert was also found to be the maximum at the 60°. Hans et al. [55] investigated with multiple V-shaped ribs as shown in Fig. 13 where they used 8 different values of relative roughness width (W/w) and found that maximum enhancement in Nusselt number at $W/w=6$ and friction factor at $W/w=10$ for the range of parameters considered. The increase in the heat transfer is due to the formation of two leading edges and two secondary flow cells with one trailing edge. Kumar et al. [59] further extended the previous authors work with V-shaped rib and investigated with multiple V shape rib with a gap as shown in Fig. 14 and concluded that the maximum enhancement in Nusselt number and Nusselt number ratio (Nu_r/Nu_s) as well as friction and friction factor ratio (f_r/f_s) occurs at relative gap width (g/e) of 1 and relative gap distance (G_d/L_v) of 0.69.Relative gap distance has more effect on increasing the heat transfer as it increases the strength of the secondary flow simultaneously the secondary flow influences the axial flow profile thus increasing the frictional effects. Singh et al. [38] investigated discrete V down ribs as shown in the Fig. 15. and found the maximum enhancement of heat transfer at $d/w=0.65$, $g/e=1$ due to high local Nusselt number development in the downstream of the gap.

6.4. Thin wires

Prasad and Saini [9] investigated the solar air heater performance with transverse thin wire as shown in Fig. 16 and found that the heat transfer coefficient increases to two times and friction factor increases to four times for the given range of parameters of the thin wire used. Gupta et al. [33] used transverse wire roughness as shown in the Fig. 10 in the underside of the absorber plate in the transitionally rough flow region to investigate the effect on thermo-physical behaviour. They found the increment of heat transfer and friction factor at the optimum values of $P/e=10$, $e/D=0.033$ and Reynolds number of 14,000. Verma and Prasad [37] investigated the effect of thin wires as the roughness element in rectangular duct similar to as shown in Fig. 10. They found that the increase in heat transfer enhancement factor (Nu_r/Nu_s) in between 1.25 and 2.08. The optimal value of roughness Reynolds number (e^+) is 24, which is equal to 71%. The cause for enhancement is artificially induced turbulence due to roughness element. Saini and Saini [47] used thin arc shaped wires as shown in Fig. 17. On the absorber plate of the solar air heater and concluded that Nusselt number decreases with the increase in relative arc angle ($\alpha/90$).

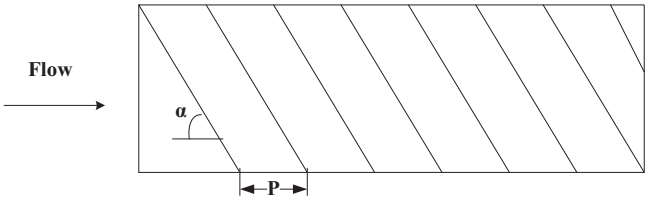

Fig. 10. Roughness element used by Gupta et al.

6.5. Expanded metal mesh

Saini and Saini [34] studied expanded metal mesh as the roughness element for the effect of long way length of mesh (l) and short way length of mesh (s) as shown in the Fig. 18 on heat transfer and pressure drop and found out the substantial increment in Nusselt number and friction factor.

6.6. Chamfered ribs

Karwa et al. [69] studied on chamfered rib as turbulator on the absorber plate as shown in Fig. 19. They concluded that the Stanton number ratio (St/St_s) and friction factor ratio (f/f_s) are maximum at the chamfer angle $\Phi=15°$ due to shedding of vortices effect. The Stanton number increase is more attributed by the generation of turbulence than increasing the surface area. The chamfered ribs increase the Stanton number and friction by 2 and 3 times in the range of parameters considered. They further concluded that the heat transfer function increases for W/H from 4.65 to and friction factor decreases for W/H from 4.67 to 7.75. The maximum enhancement in Nusselt number (Nu) and friction factor (f) of various geometries is enlisted in Table 3.

6.7. Wedge shaped ribs

Bhagoria et al. [70] investigated on wedge shaped ribs as shown on the Fig. 20. They concluded that the Nusselt number attains

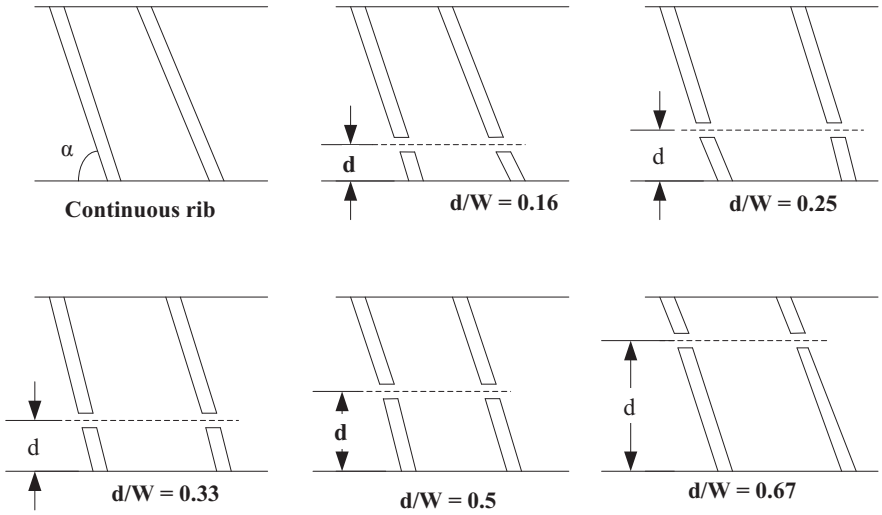

Fig. 11. Various types of inclined ribs used by Aharwal et al.

maximum at $P=7.57$ and wedges shaped transverse ribs helps in separation and forming a wide shear layer which reattaches at $P=6$–8. The maximum Nusselt number and friction factor was found to be of 2.4 and 2.8 respectively for the range of parameters investigated. They further concluded that the Nusselt number is maximum at the wedge angle of 100.

6.8. Metal grit ribs

Karmare and Tikekar [52] investigated the absorber plate of the solar air heater with metal grit as roughness element as shown in Fig. 21. They found that the effective efficiency increases at Reynolds number from 8890 to 17,030 at higher insulation for the range of parameters investigated.

6.9. Dimpled surface

Saini and Verma [46] investigated the effect of flow and roughness parameters on the solar air heater with dimpled shaped surface on the absorber plate as shown in Fig. 22. They concluded that friction factor is minimum for $P/e=10$ and maximum Nusselt number occurs at $e/D=0.037$ and $P/e=10$ for the given range of parameters selected. Sethi et al. [62] investigated the dimple shaped roughness element on the absorber plate in arc shaped as shown in the Fig. 23. They concluded that the maximum heat transfer occurs at P/e of 10 due to flow separation and reattachment in these types of surfaces.

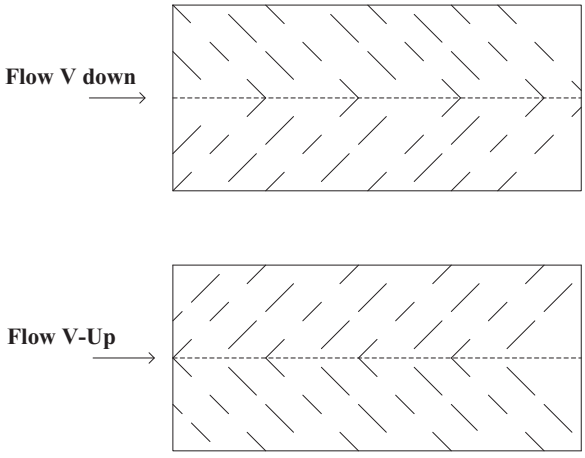

Fig. 12. Roughness element used by Mulluwork et al.

6.10. W shaped ribs

Lanjewar et al. [58] investigated the thermo-physical behaviour of the W-shaped ribs of different orientation on the absorber plate as shown in Fig. 24. They concluded that W down ribs give the higher thermo-hydraulic performance $(Nu_r/Nu_s)/(f_r/f_s)$ at e/D of 0.03375, P/e of 10 and α of 60°. They further concluded that the W down ribs were better than W up ribs. They also made the study on W-shaped ribs with increment in Nusselt number and friction factor of 2.36 and 2.01.

6.11. Surface protrusion

Bhusan and Singh [61] investigated the solar air heater with protrusion on the absorber plate as shown in Fig. 25. They concluded that the heat transfer coefficient increases as compared to smooth surface, which may be due to main flow impingement, vortex generation on both sides of the protrusion and flow separation. The performance is highest at relative short way length (S/e) of 31.25 and relative long way length (L/e) of 31.25. Yadav et al. [67] investigated the solar air heaters with circular protrusions in arc shape for the various ranges of parameters. They concluded that the maximum heat transfer and friction factor occurs at relative roughness $(e/D)=0.03$, relative roughness pitch $(P/e)=12$ and arc angle $(\alpha)=60°$.

6.12. U shaped ribs

Bopche and Tandale [53] investigated for the thermo-hydraulic performance of solar air heaters with inverted U shaped ribs on the absorber plate as shown in Fig. 26. They concluded that their roughness element is efficient in heat transfer even at lower Reynolds number ($Re<5000$). They further concluded that the turbulence is created only in the viscous sub layer resulting in higher thermo-hydraulic performance than smooth solar air heaters.

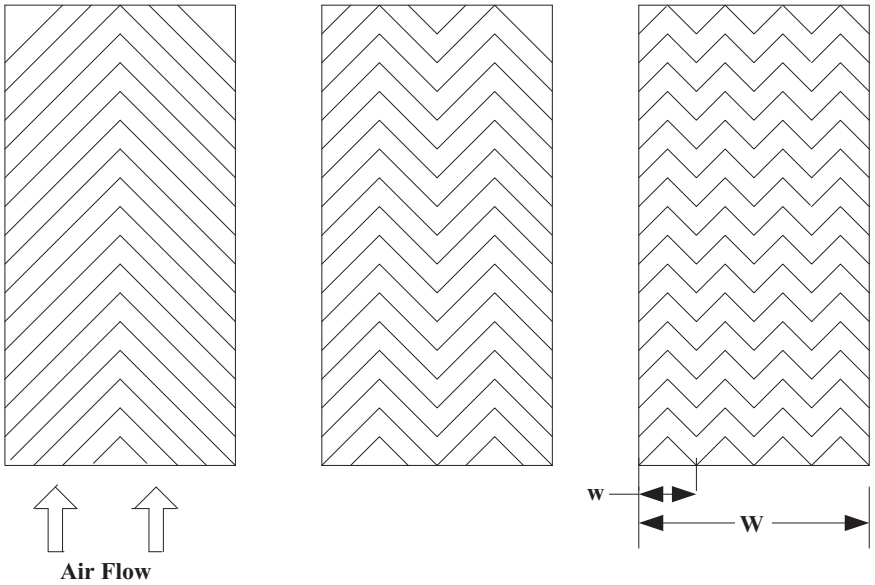

Fig. 13. Multiple V ribs used by Hans et al.

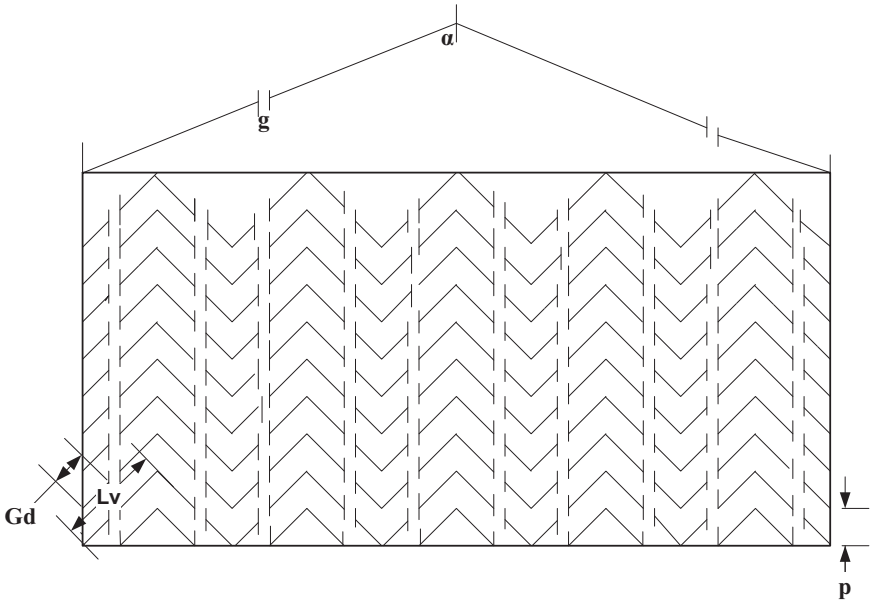

Fig. 14. Multi V shape with gap ribs used by Kumar et al.

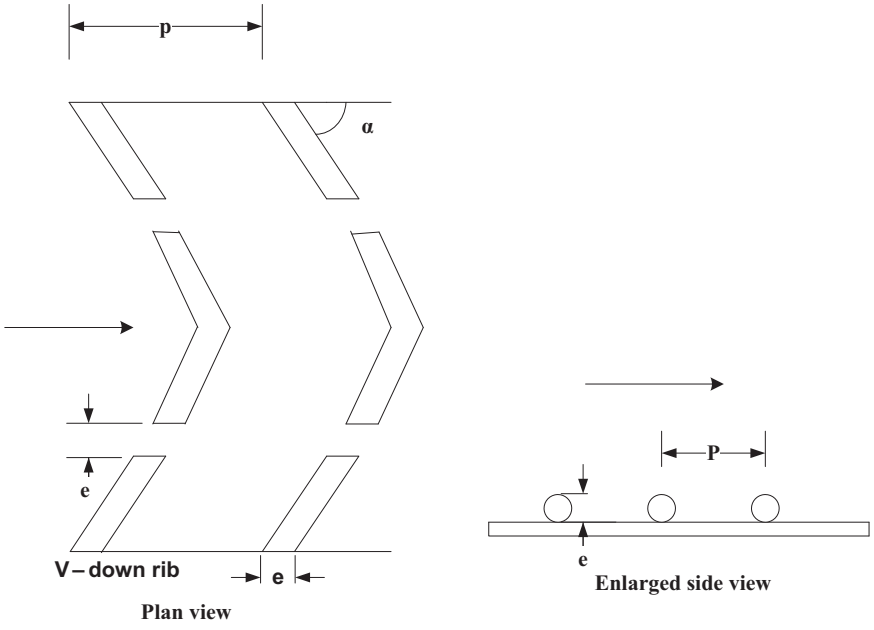

Fig. 15. Discrete V-down rib arrangement used by Sukhmeet et al.

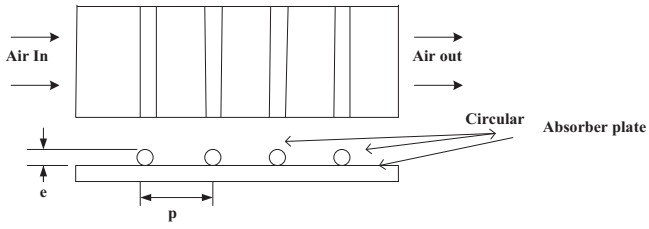

Fig. 16. Transverse ribs used by Prasad and Saini.

6.13. Compound ribs

Various authors have investigated on the combinations of different ribs on the absorber of solar air heaters and to know the flow and heat transfer characteristics with a range of parameters selected. Jaurker et al. [42] investigated the solar air heaters with the combination of rib and groove on the absorber plate as shown in the Fig. 27. They concluded that the rib – groove combination giver higher heat transfer as compared to the ribbed surface for which the vortices formed around the groves are responsible. The maximum increase in Nusselt number and friction factor is at $P/e=6$, and $g/p=0.4$ when compared to smooth solar air heaters for the range of the parameters selected. Varun et al. [54] investigated the combination of transverse and inclined ribs as shown in Fig. 28 and they concluded that the maximum thermal efficiency has been found to be at P/e of 8. Layek et al. [48] investigated the solar air heaters with the combination of rib and groove on the absorber plate as roughness elements as shown in Fig. 29. They concluded that the increase in the Nusselt number and the friction factor is due to more frequently shedding of vortices with chamfering of the ribs and generation of an additional vortex by the grooves causes higher heat removal from the surface as well as higher frictional loss as compared to square rib

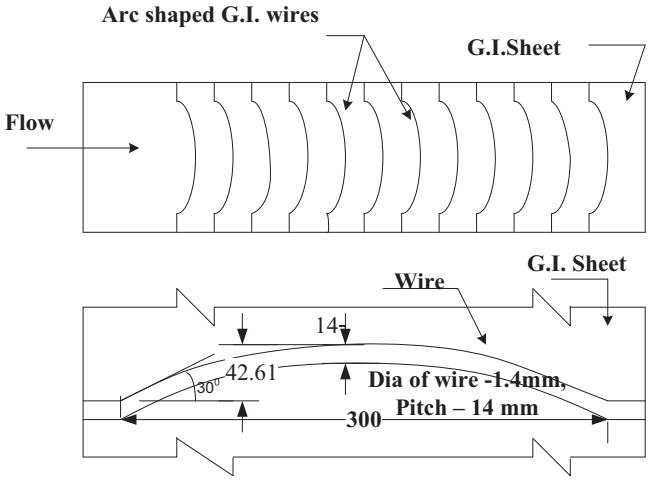

Fig. 17. Roughness elements used by Saini & Saini.

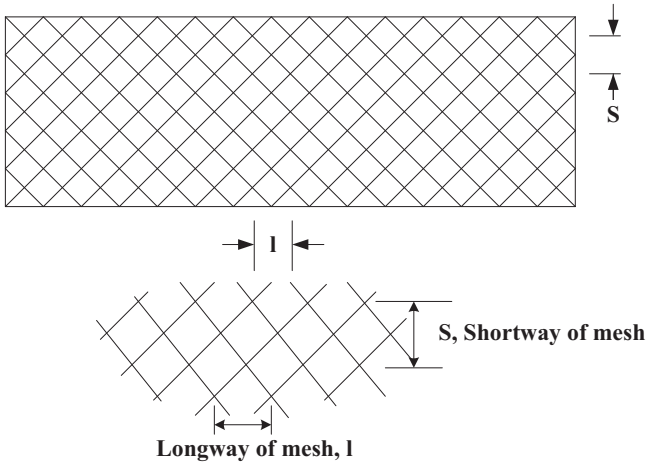

Fig. 18. Expanded metal mesh used by Saini and Saini.

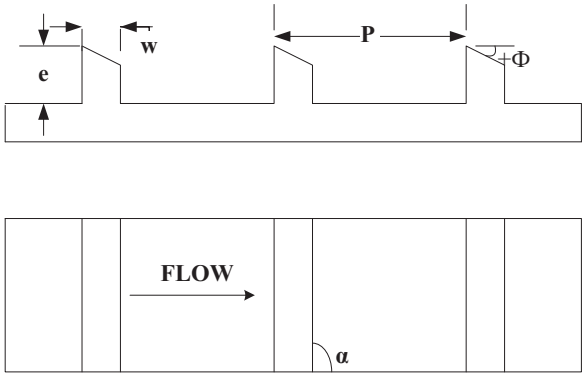

Fig. 19. Chamfered rib geometry used by Karwa et al.

and groove combination. The optimum performance for these combinations occurs at $\alpha = 18^{\circ}$ and increment in Nusselt number lies between 2 and 2.6 for the range of parameters considered.

7. Materials used for artificial rib roughness and absorber plates

Different materials have been used for absorber plate and artificial roughness geometry in solar air heaters and ducts so far. Most of the researchers [2,9,46,47,64,55–59,65] have used galvanized iron sheet of with conductivity of 18 W/mK of different gauges for the absorber plate. Few researchers [11,48,62,72,73] have used aluminium sheets which has conductivity of 205 W/mK as absorber plate in solar air heaters. Tanda [27] and Gupta et al. [71] used stainless steel with conductivity of 16 W/mK as absorber plate material in his experimentation. Gill et al. [74] have used fibre glass sheet as absorber plate for low cost solar air heaters. As far as artificial roughness or rib materials are concerned the authors have used high conductivity materials preferably with few exceptions. Han [14] used brass as rib material which has conductivity of 109 W/mK. Many researchers [59,55,72] have used various aluminium wires as roughness rib elements. The use of high conducting material is to keep the temperature of rib geometry at the same temperature as that of plate [11]. However Tanda [27] used balsa wood with very low conductivity of 0.048 W/mK for making roughness rib elements. Use of balsa wood is to reduce conduction effects in the heat transfer process.

Table 3
Maximum enhancement in values of Nusselt number and friction factor.

S. no.	Authors	Roughness element	Enhancement in Nu and f	
			Nu	f
1.	Prasad and Saini [9]	Small diameter protrusion wire	2.38	4.25
2.	Saini and Saini [34]	Expanded metal mesh	4	5
3.	Singh et al. [73]	V down rins	3.04	3.11
4.	Bhagoria et al. [70]	Wedge shaped ribs	2.4	5.3
5.	Momin et al. [39]	V-shaped continuous wire rib	2.30	2.83
6.	Chandra [26]	One ribbed wall	2.43	3.14
		Two ribbed walls	2.64	5.39
		Three ribbed walls	2.81	3.14
		Four ribbed walls	2.99	9.5
7.	Karwa [40]	Transverse rib	2.30	3.42
		Inclined ribs	2.12	3.92
		V continuous ribs	2.37	3.65
		V discrete ribs	2.47	2.47
8.	Jaurker [42]	Rib and groove combination	2.75	3.61
9.	Aharwal et al. [45]	Inclined continuous with gap ribs	2.95	2.87
10.	Saini and Saini [47]	Arc shaped wire ribs	3.80	1.75
11.	Layek et al. [48]	Chamfered compound rib	2.6	3.35
12.	Kumar et al. [49]	Discritized W shape rib	2.16	2.75
13.	Aharwal et al. [50]	Integral inclined discrete rib	2.83	3.60
14.	Bopche and Tandale [53]	U shaped rib	2.82	3.72
15.	Saini and Verma [46]	Dimple shape	7.58	4.68
16.	Hans et al. [55]	Multiple V shape rib	6.0	5.0
17.	Lanjewar et al. [56]	W shaped rib	2.36	2.01
18.	Bhusan et al. [61]	Protrusion	3.8	2.2
19.	Singh et al. [63]	Discrete V shape ribs	3.04	3.11
20.	Kumar et al. [59]	Multi V shape with gap rib	6.32	6.12
21.	Kumar et al. [64]	Multi V shape with gap rib	6.74	6.37
22.	Prasad [65]	GI wires of varying diameter	55	
23.	Yadav et al. [67]	Circular protrusions in arc shape	2.89	2.93

8. Thermo hydraulic performance $[\{(Nu_r/Nu_s)/(f_r/f_s)\}^{1/3}]$

Thermo-hydraulic performance measurement is an important criterion to judge the performance of solar air heaters. Artificial roughness is employed to increase the heat transfer from the surface. Though the use of artificial roughness in absorber plate substantially increases the heat transfer, it also causes substantial increase in the pressure drop due to friction which needs to be restricted to the possible minimum value. To measure the relevance of use of artificial roughness on absorber plate of solar air heater or duct, the thermo hydraulic performance measurement is

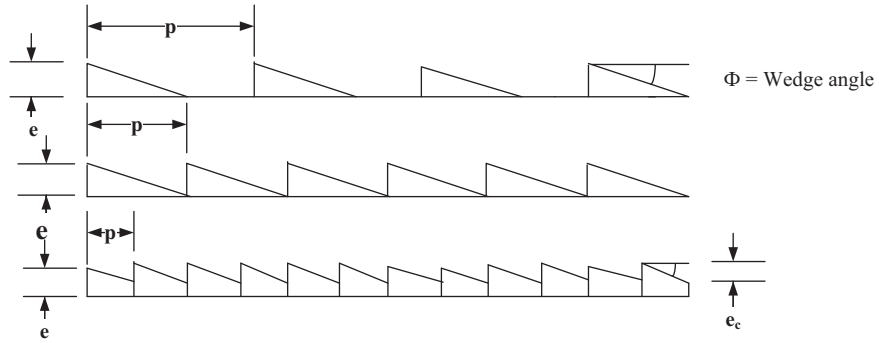

Fig. 20. Rib geometries used by Bhagoria et al.

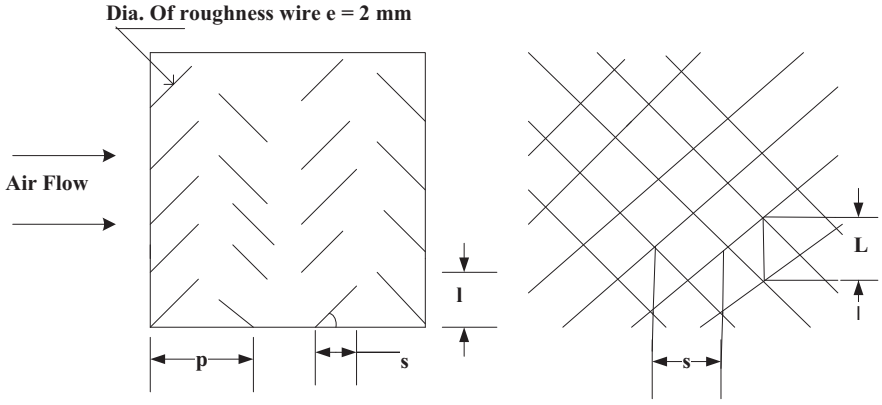

Fig. 21. Roughness element used by Karmare and Tikekar.

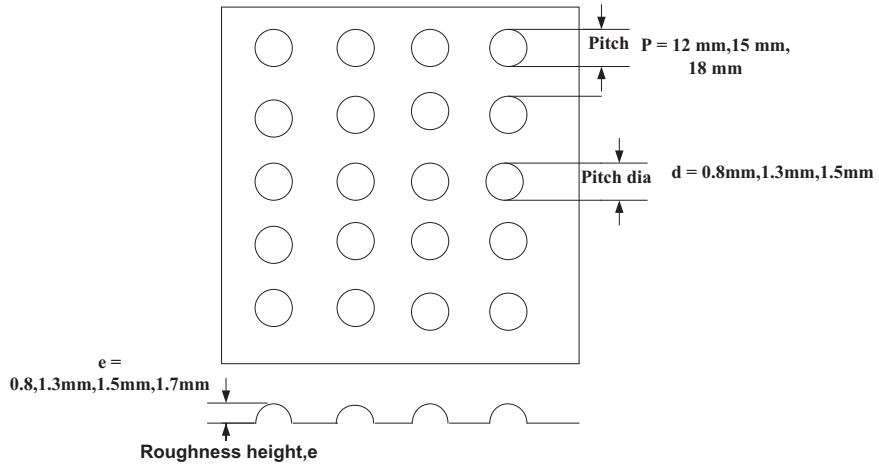

Fig. 22. Rib geometry used by Saini and Verma.

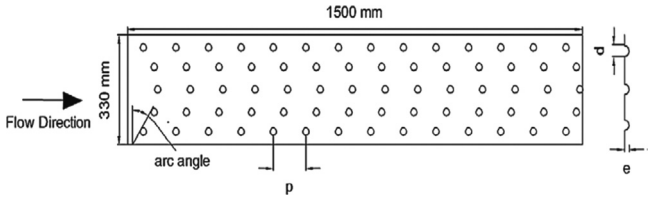

Fig. 23. Dimple in arc shape by Muneesh et.al.

done. This can be fulfilled by considering the heat transfer and the friction factor characteristics simultaneously. The parameter that facilitates simultaneous consideration of thermal and hydraulic performance is given by Webb and Eckert [7] as $(Nu_r/Nu_s)/(f_r/f_s)^{1/3}$ which is called thermo-hydraulic parameter. This parameter is in fact is the ratio of Nusselt number ratio of roughened surface to smooth surface and friction factor ratio of roughened surface to smooth surface. The higher value, greater than one i.e. (>1) of this parameter is always desirable for justifying the use of artificial roughness in the solar air heaters or duct. The higher the value the better is the performance of the artificially roughened solar air heaters. It shows the comparative increase in the Nusselt number to the friction factor of roughened surface in comparison with the smooth surface without roughness elements. The value of the thermo hydraulic parameter calculated in the experimental studies of solar air heaters by various researchers with artificial roughness so far ranges from 1.38 to 2.39. This parameter is also used to compare the performance of various roughness elements arrangement combinations to obtain the best one. Various authors

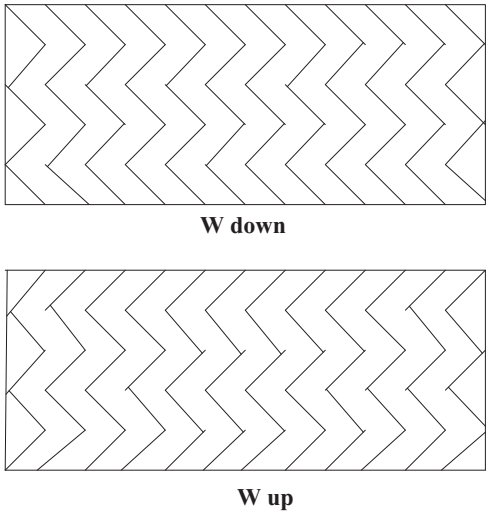

Fig. 24. Rib geometry used by Lanjewar et al.

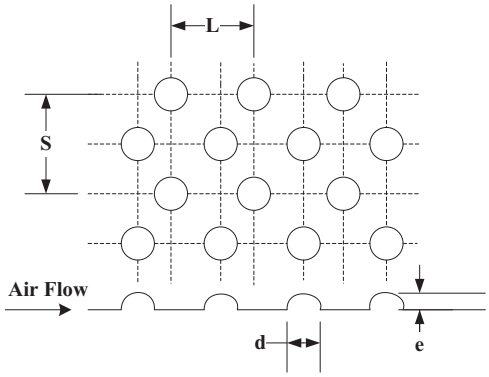

Fig. 25. Rib geometry used by Bhusan and Singh.

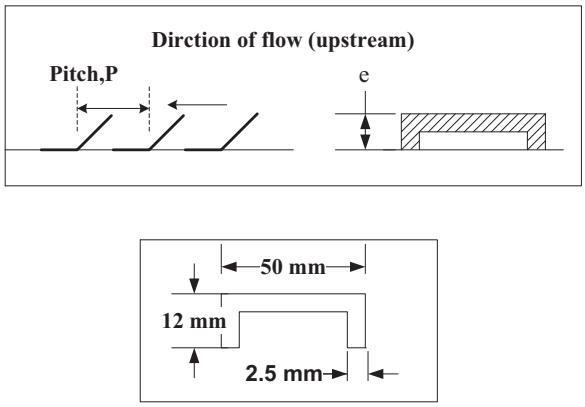

Fig. 26. Roughness element used by Bopche and Tandale.

who conducted experiments and measured the thermo hydraulic performance parameter in their work are enlisted in Table 4.

9. Correlations for Nusselt number (Nu) and friction factor (*f*)

Initially, Nikuradse [5] developed the friction correlations for sand grain roughness using the law of the wall similarity covering a wide range of e/D_h values, which was applicable to any geometrically similar roughness. Dipprey and Sabersky [6] then developed the heat transfer similarity law for flow in sand grain roughened tube using the wall similarity law applicable to velocity profile as suggested by Nikuradse, assuming the law of wall similarity to be applied for temperature profiles also for geometrically similar roughness. Then Webb using Nikuradse's law of wall similarity and heat momentum transfer analogy developed friction correlation for turbulent tube flow with repeated ribs by taking into consideration the geometrically non similar roughness parameter, the relative roughness pitch P/e [7]. Further, the concept was applied by the researchers to develop the correlations of heat transfer and friction factor for turbulent flow between parallel plates with repeated rib roughness by taking into account the geometrically non similar roughness parameters like relative roughness pitch P/e, rib shape and flow attack angle (α). The other researchers incorporated other geometrical parameters and flow conditions as well for deriving these correlations showing that the Nusselt number and friction factor depends on all geometrical parameters and flow conditions selected for the experimental work. Correlations are used to predict the thermo-hydraulic performance for any particular application. These general correlations developed for the friction factor and heat transfer coefficient covering a wide range of data are necessary to study the useful results of the roughened surfaces. These statistical correlations also help to determine optimum geometrical parameters like relative roughness pitch (P/e), relative roughness height (e/D_h), angle of attack (α) and flow parameters like Reynolds number (Re) used for the application. These correlations help the designers and investigators to understand the significance of these geometrical and flow parameters within the range selected in their research work. All the correlations show that the Nusselt number and friction factor strongly depend on the non dimensional parameters considered during their experimental work. These correlations are developed on the basis of regression analysis of the experimental data obtained in their work. The different correlations developed by various authors using the range of parameters selected in their work are shown in Table 5.

10. Discussion

The review of the literatures on experiments with artificial roughness rib elements in ducts and solar air heaters reveals that these small height elements when used, increases the heat transfer substantially but with the adverse effect of increase in frictional losses. Thus, an external pumping medium is required to overcome the frictional forces. These elements can be of various shapes and geometry like triangular, square, V Shape, W shape, thin wires, wire mesh, grooves, protrusions and rib and grooves etc which are attached to the surface or generated by machining. The various geometrical and flow parameters of these elements like roughness height (e), relative roughness pitch (P/e), relative roughness height (e/D_h), angle of attack (α), aspect ratio (W/H) of the duct or solar air heaters and Reynolds number (Re) play an important role in determining the heat transfer and the friction factor characteristics of the flow process. These elements create turbulence in laminar sub layer close to the surface and break the boundary layer to increase the heat transfer. The geometrical parameters of each element used has been enlisted in Table 1. The optimum performance parameters of these elements has also been enlisted in Table 2.The study reports that the protrusions or dimples generated on the surface has lesser friction factor as compared to increase in Nusselt number than elements which have been attached to the surface. The inclined parallel ribs on the absorber surface give optimum performance at 45°. The various statistical correlations which have been developed by various researchers can be used to understand the effect of geometrical parameters on thermo hydraulic behaviour. These elements have also been evaluated on the basis of thermo hydraulic parameter

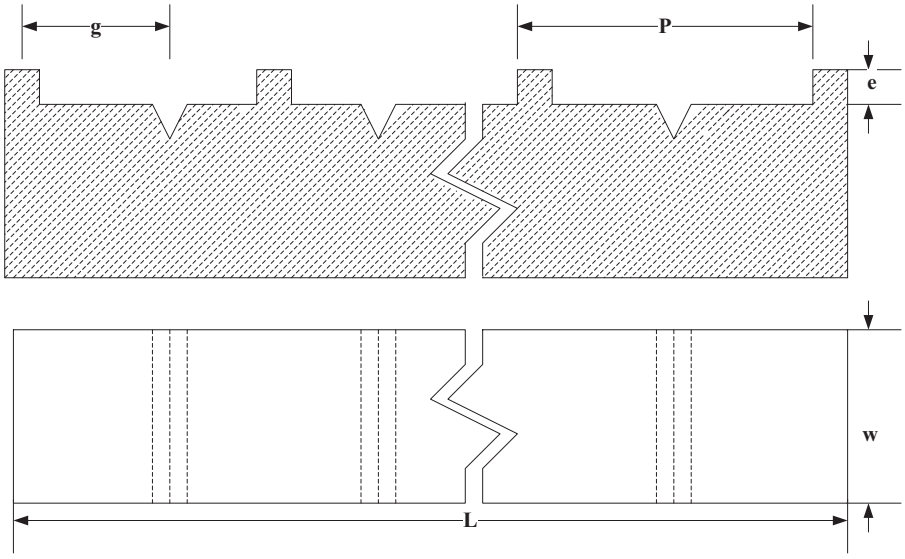

Fig. 27. Combination of rib and groove by Jaurker et al.

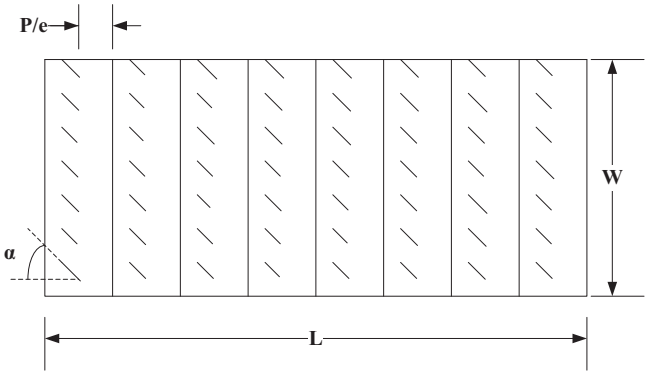

Fig. 28. Combination of the inclined and the transverse ribs by Varun et al.

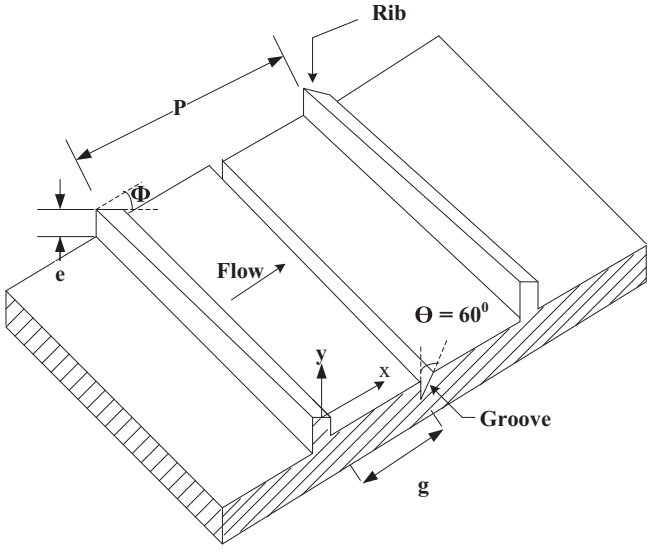

Fig. 29. Combination of rib and groove by Layek et al.

which measures the effectiveness of use of these elements and is enlisted in Table 4.On the basis of this review a comparative study has been made regarding the use of these elements for heat transfer enhancement in ducts and solar air heaters.

Table 4
Values of thermo-hydraulic performance parameters.

Authors	Roughness element	$[\{(Nu_r/Nu_s)/(fr/fs)\}^{1/3}$
Prasad and Saini [9]	Transverse wire	1.78
Bhagoria et al. [70]	Transverse wedge shaped ribs	1.38
Jaurker et al. [42]	Rib groove	1.76
Saini and Saini [34]	Expanded metal mesh	2.34
Karmare and Tikekar [44]	Metal grit ribs	2.39
Bopche and Tandale [53]	Inverted U shape rib	1.82
Lanjewar et al. [58]	W shape rib of different orientations	1.98

11. Conclusion

In this paper an attempt has been made to account for the various experimentation works in ducts and solar air heaters with artificial roughness rib element and its effect on the heat transfer and the friction factor characteristics. Different types of elements, materials and geometrical parameters have been used to evaluate the thermo-hydraulic performance of the ducts and solar air heaters.

On the basis of the literature review the following conclusions are drawn:

1. There is a definite increase in heat transfer in solar air heaters with increase in friction to the flow when its surface is roughened. However, the different investigators find different values of increment in heat transfer and friction factor for each type of rib geometry used.
2. The maximum heat transfer enhancement in terms of Nusselt number (Nu) and friction factor (f) of 7.58 and of 4.68 is found in the investigations of Saini and Verma [46] followed with multi V shape with a gap as the roughness element by Kumar et al. [64] of 6.74 and 6.37 and multiple V shape ribs by Hans et al. [55] of 6 and 5.It is observed that the increase in heat transfer is achieved, but the friction factor is also increasing simultaneously. The maximum enhancement in Nusselt number and friction factor is enlisted in Table 3.
3. As far as different rib geometries in experiments studied so far, the protrusions or dimple shape elements offers minimum friction factor value when compared to increase in the Nusselt

Table 5
Nusselt number and friction factor correlations developed for various geometries in solar air heaters.

Element type	Authors	Parameters and range	Heat transfer correlation	Friction factor correlation
Transverse ribs	Hong and Hsieh [21]	e/D_h=0.19	$Nu = 0.056Re_H^{0.74}$ (forTu = 0.04) $Nu = 0.03\ Re_H^{0.79}$(forTu = 0.07) $Nu = 0.019\ Re_H^{0.83}$(for Tu = 0.07)	
Small diameter protrusion wire	Prasad and Saini [9]	P/e=5.31 e/D_h=0.020–0.033	$\overline{St} = \bar{f}/2/1+\sqrt{f/2}\left\{\frac{4.5(e^+)^{0.28}}{Pr^{0.57}-0.95(P/e)^{0.53}}\right\}$	$f_r = 2/[0.95(p/e)^{0.53} + 2.5\ In(D/2e) - 3.75]^2$
Small diameter traverse rib	Gupta et al. [35]	P/e=10–20 Re=500–50,000 e/D=0.018–0.52Re=3000–18,000	$Nu = 0.000824(e/D)^{-0.178}(W/H)^{0.284}Re^{1.062} \le 35$ $Nu = 0.000307(e/D)^{-0.469}(W/H)^{0.245}Re^{1.062} \ge 35$	$f = 0.06412(e/D)^{0.019}(W/H)^{0.237}Re^{-0.185}$
Small diameter transverse protrusion wire	Verma and Prasad [37]	e/D=0.01–0.03	$Nu = 0.08596(P/e)^{-0.54}(e/D)^{0.072}Re^{0.723}\ e \le 24$ $Nu = 0.0245(P/e)^{-0.016}(e/D)^{0.021}Re^{0.802}\ e \ge 24$	$f = 0.0245(P/e)^{-0.0206}(e/D)^{0.021}Re^{-1.25}$
V-Shaped wire ribs and V-shaped inclined wire ribs	Gupta [75]	P/e=10–40 e^+=8–42 Re=5000–20,000 e/D=0.02–0.053	$Nu = 0.00824(e/D)^{-0.178}(W/H)^{0.284}Re^{1.062}$ $\exp[-0.04(1-\alpha/60)^2](k/D)\ e \le 35$ $Nu = 0.00307(e/D)^{-0.469}(W/H)^{0.245}Re^{8.812}$ $\exp[-0.475(1-\alpha/60)^2](k/D)\ e \ge 35$	$f = 0.06412(e/D)^{0.019}(W/H)^{0.0237}Re^{-0.185}$ $\exp[-0.0993(1-\alpha/60)^2]$
V-Shaped staggered discrete wire ribs	Mulluwork et al. [68]	P/e=7.5–10, α=300–900 Re =5000–20,000 e/D=0.02	$Nu = 0.00534(B/S)^{1.3496}Re^{1.2991}$	$f = 0.7117(B/S)^{0.0636}Re^{-2.991}$
V-shaped continuous wire rib	Momin et al. [39]	B/S=3–9 α=600 Re=2000–15,500 e/D_h=0.02–0.034	$Nu = 0.067(e/D)^{0.424}(\alpha/60)^{-0.077}Re^{0.888}$ $\exp[-0.0782\ In(\alpha/60)^2]$	$f = 6.266(e/D)^{0.565}(\alpha/60)^{-0.093}Re^{-0.425}$ $\exp[-0.719\ In(\alpha/60)^2]$
Inclined, discrete and continuous wire rib	Karwa [40]	P/e=10 α=300–900 Re=2500–18,000 e/D_h=0.467–0.05	$G = 32.2\ e^{-0.006}(W/H)^{0.5}(P/e)^{2.56}$ $\exp[0.7343\ In\ (p/e)^2](e^+)^{0.08}$	$f = 1.66e^{-0.0078}(W/H)^{-0.4}(P/e)^{0.2695}$ $\exp[-0.719\ In(P/e)^2(e^+)^{-0.075}]$ For $7 \le e^+ \le 20\ R$ $f = 1.325e^{-0.0078}(W/H)^{-0.4}(P/e)^{0.2695}$ $\exp[-0.719\ In\ (P/e)^2(e^+)^{-0.075}]$ For $20 \le e^+ \le 60\ R$
Wire ribs-grid shape	Karmare and Tikekar [44]	P/e=10 α=600–900 B/S=3 W/H=7.19–7.75 Re=2500–18,000 e/D_h=0.035–0.044	$Nu = 2.4(e/D_h)^{0.42}(l/s)^{-0.146}\ Re^{1/3}$ $(P/e)^{-0.27}$	$f = 15.55(e/D_h)^{0.94}(l/s)^{-0.27}Re^{-0.26}(P/e)^{-0.51}$

Table 5 (*continued*)

Element type	Authors	Parameters and range	Heat transfer correlation	Friction factor correlation
Inclined and transverse ribs	Aharwal at el. [50]	$P/e=12.5–36$ $l/s=1.72–1$ Re=4000–17,000 $e/D_h=0.0377$	$Nu=0.0102(e/D)^{0.51}Re^{1.148}$ $[\{1-(0.25-d/w)^2\{0.01(1-g/e)^2\}\}]$	$f=0.5(e/D)^{0.72}Re^{-0.0836}$
Inclined and transverse wire ribs	Varun et al. [72]	$P/e=10$ $\alpha=600$ $d/w=0.167–0.5$ $W/H=5.87$ Re=3000–18,000 $P/e=10$ $e/D_h=0.030$ Re=2000–20,000	$Nu=0.0006(P/e)^{0.0104}Re^{1.213}$	$f=1.0858(P/e)^{0.0114}Re^{-0.3685}$
Arc shaped wire ribs	Saini and Saini [47]	$g/e=0.5–2$	$Nu=0.001047(e/D)^{0.3772}$ $(\alpha/90)^{-0.1198}Re^{1.123}$	$f=0.14408(e/D)^{-0.1765}(\alpha/90)^{0.1185}Re^{-0.17103}$
Multiple V shaped ribs	Hans at el. [55]	$P/e=10$ $\alpha/90=0.333–0.666$ $d/w=0.167–0.5$ W/H=5.87 Re=2000–17,000 $P/e=6–12$	$Nu=3.35\times10^{-5}Re^{0.92}(e/D)^{0.77}(W/w)^{0.43}$ $(\alpha/90)^{-0.49}\exp[-0.1177(L_n(W/w))^2]$ $\exp[-0.61(L_n(\alpha/90))^2](P/e)^{8.54}$ $\exp[-2.040(L_n(P/e))^2]$	$f=4.47\times10^{-4}Re^{-0.3188}(e/D)^{0.73}(W/w)^{0.22}(\alpha/90)^{-0.39}$ $\exp[-0.52(L_n(\alpha/90))^2](P/e)^{8.9}$ $\exp[-2.133(L_n(P/e))^2]$
Expanded metal mesh	Saini and Saini [34]	$e/D=0.0213–0.0422$ $\alpha=300–750$ $W/w=1–10$ Re =2000–20,000 $l/e=25–71.87$	$Nu=4.0\times10^{-4}Re^{1.22}(e/D)^{0.625}(s/10e)^{2.22}$ $\exp[1.25(In(s/10e))^2](l/10e)^{2.66}$ $\exp[0.824(In(l/10e))^2]$	$f=0.815Re^{0.316}(l/e)^{0.266}(s/10e)^{0.19}Re^{-0.26}(10e/d)^{0.591}$
Discrete V shaped	Singh et al. [73]	$s/e=15.62–46.87$ $e/D_h=0.012–0.0390$ Re=1900–13,000 $P/e=4–12$	$Nu=2.36\times10^{-5}Re^{0.90}(P/e)^{3.5}(\alpha/60)^{-0.023}$ $(g/e)^{-0.014}(e/D_h)^{0.47}$ $\exp(-0.84(l_n(p/e))^2)$ $\exp((-0.72(l_n(\alpha/60))^2))$ $\exp((-0.05(L_n(d/w))^2))$ $\exp((-0.15(l_n(g/e))^2))$	$f=44.13\times10^{-2}Re^{-0.126}(P/e)^{2.74}(\alpha/60)^{-0.034}(d/w)^{-0.058}(g/e)^{-0.031}(e/D_h)^{0.70}$ $\exp(-0.685(l_n(P/e))^2)\exp((-0.93(l_n(\alpha/60))^2))$ $\exp((-0.058(L_n(d/w))^2))\exp((-0.21(l_n(g/e))^2))$
		$g/e=0.5–2$ $\alpha=300–750$ $d/w=0.2–0.8$ $e/D_h=0.015–0.043$ Re =3000–15,000		

Machined ribs	Karwa et al. [69]	P/e=4.5–8.5	$G = 103.77\, e^{-0.006}(W/H)^{0.5}(P/e)^{2.56}$ $\exp[0.7343 \ln (P/e)^2](e^+)^{-0.31}$ For $7 \le e^+ \le 20$ $G = 32.26\, e^{-0.006}(W/H)^{0.5}(+/e)^{2.56}$ $\exp[0.7343 \ln (P/e)^2](e^+)^{0.8}$ For $20 \le e^+ \le 60$	$f = 1.66e^{-0.0078}(W/H)^{-0.4}(P/e)^{0.2695}$ $\exp[-0.762 \ln (P/e)^2(e^+)^{-0.075}]$ For $7 \le e^+ \le 20$ R $f = 1.325e^{-0.0078}(W/H)^{-0.4}(P/e)^{0.2695}$ $\exp[-0.762 \ln (P/e)^2(e^+)^{-0.075}]$ For $20 \le e^+ \le 60$ R
Wedge shaped ribs	Bhagoria et al. [70]	e/D_h=0.014–0.0320 d/w=0.167–0.5 W/H=5.87 Re =3000–20,000 P/e=60.17$\Phi^{-1.0264}$ < P/e 12.12	$\mathrm{Nu} = 1.89 \times 10^{-4}\, \mathrm{Re}^{1.21}(e/D)^{0.426}(P/e)^{2.94}$ $\exp[-0.71 (\ln(P/e))^2](\Phi/10)^{-0.018}$ $\exp[-1.50 (\ln(\Phi/10))^2]$	$f = 12.44\, \mathrm{Re}^{-0.18}(e/D)^{0.99}(P/e)^{-0.52}\mathrm{Re}^{-0.26}(\Phi/10)^{0.49}$
Chamfered rib groove combination	Layek et al. [48]	Φ=8–150 e/D=0.015–0.033 Re=3000–18,000 P/e =4.5–10	$\mathrm{Nu} = 0.00206\, \mathrm{Re}^{0.936}\, (e/D)^{0.349}(P/e)^{30318}$ $\exp[-0.868 (\ln(P/e))^2](g/p)^{1.108}$ $\exp[2.486\{\ln(g/p)\}^2 + 1.406\{\ln(g/p)\}^3]$	$f = 0.001227\, \mathrm{Re}^{-0.199}\, (e/D)^{0.585}(P/e)^{7.19}$ $\exp[-1.854\, \{\ln(P/e)\}^2](g/p)^{0.645}\, \exp[1.513\{\ln(g/p)\}^2 + 0.8662\{\ln(g/p)\}^3]$
Dimple protrusions	Saini and Verma [46]	Φ=5–300 e/D=0.022–0.04 Re=3000–18,000 g/p=0.3–0.6 e/D_h=0.018–0.037	$\mathrm{Nu} = 5.2 \times 10^{-4}\, \mathrm{Re}^{1.27}(e/D)^{0.33}(P/e)^{3.15}$ $\exp[-2.2\, \{\log (P/e)\}^2]$ $\exp[-1.30\, \{\log (e/D)\}^2]$	$f = 0.0642\, \mathrm{Re}^{-0.423}(e/D)^{-0.0214}(P/e)^{-0.465}$ $\exp[0.054\, \{\log (P/e)\}^2]\, \exp[-0.840\, \{\log (e/D)\}^2]$
Dimple shaped Roughness	Bhusan and Singh [61]	Re=2000–12,000 P/e=8–12 L/e=25–37.5	$\mathrm{Nu} = 2.1 \times 10^{-88}\, \mathrm{Re}^{1.452}(S/e)^{12.94}\, (L/e)^{99.2}$ $(d/D)^{-3.9}\exp[-10.4 (\log (S/e))^2]$ $\exp[-77.2 (\log (L/e))^2]$ $\exp[-7.83 (\log (d/D))^2]$	$f = 2.32\mathrm{Re}^{-0.201}(S/e)^{-0.383}\, (L/e)^{-0.484}\, (d/D)^{0.133}$
Multi V shape with gap rib	Kumar et al. [64]	S/e=18.75–37.5 e/D_h=0.03 d/D=0.147–0.367 Re =1900–13,000 P/e=6–12	$\mathrm{Nu} = 8.534 \times 10^{-3}\, \mathrm{Re}^{-0.932}(e/D)^{0.175}(W/w)^{0.506}$ $\exp[-0.753 (In(W/w))^2](G_d/L_v)^{-0.0348}\, \exp[-0.0653(Ln(G_d/L_v))^2\ ]\, (g/e)^{-0.0708}$ $\exp[-0.223 (In(g/e))^2](\alpha/60)^{-0.0239}\ \exp[0.1153 (In(\alpha/60))^2](P/e)^{1.196}$ $\exp[-0.2805 (In(P/e))^2]$	$f = 3.1934\mathrm{Re}^{-0.3.51}(e/D)^{0.268}(W/w)^{0.1132}$ $\exp[-0.974 (In(W/w))^2](G_d/L_v)^{0.0610}\exp[-1.065 (In((G_d/L_v)^2))^2](g/e)^{-0.1769}$ $\exp[-0.6349 (In(g/e))^2](\alpha/60)^{0.1553}\exp[-0.1527 (In(\alpha/60))^2](P/e)^{0-0.7941}$ $\exp[0.1486 (In(P/e))^2]$
Circular protrusions	Yadav et al. [67]	g/e=0.5–1.5 e/D=0.022–0.043 W/w=1–10 G_d/L_v=0.24–0.80 α=300–750 Re=2000–20,000 P/e=12–24	$\mathrm{Nu} = 0.154\, \mathrm{Re}^{1.017}\, (P/e)^{-0.38}\, (e/D)^{0.521}\, (\alpha/60)^{-0.213}$ $\exp[-2.0233 (In(\alpha/60))^2]$	

Table 5 (*continued*)

Element type	Authors	Parameters and range	Heat transfer correlation	Friction factor correlation
		$e/D=0.015–0.03$ $W/H=11$ $\alpha=450–750$ $Re=3600–18,100$		$f=7.207\ Re^{-0.56}\ (P/e)^{-0.18}\ (e/D)^{0.176}\ (\alpha/60)^{0.038}$ $\exp[-1.412\ (ln(\alpha/60))^2]$

number value at the optimum value of parameters selected than other rib elements.

4. In transverse rib elements, most of the experiments conducted gives the result that the performance of the V shaped, W shaped ribs is optimum at flow attack angle of 60° whereas for transverse inclined ribs the optimum performance angle of inclination is 45°.
5. The experiments of artificial roughness in solar air heater with different rib geometry parameters give the optimum performance at certain values of the parameters. The optimum values of the parameters of each rib element are enlisted in Table 2.
6. The various correlations developed for the Nusselt number and friction factor for the range of parameters considered will give insight to the designers and other investigators in their work for finding out the optimum values. These correlations and heat transfer values can help the beginners of this field to know about the various geometries used, until now, and help them to understand the effect of each parameter on the heat transfer and flow characteristics.
7. The metal grit ribs are the most suitable rib element in terms of thermohydraulic performance parameter.
8. High aspect ratio values have better heat transfer efficiency whereas low aspect ratio values have better heat transfer performances in solar air heaters and ducts.

References

[1] Hsieh JS. Solar energy engineering. New Jersey: Prentice Hall; 1986.
[2] Gupta CL, Garg HP. Performance studies on solar air heaters. Sol Energy 1967;11:25–31.
[3] Varun Saini RP, Singal SK. A review of roughness geometry used in solar air heaters. Sol Energy 2007;81:1340–50.
[4] Tiwari GN. Solar energy. Fundamentals, Design, Modelling and Application. Narosa Publications; 2008.
[5] Nikuradse J. Laws for flow in rough pipes. VDI - Forschungsheft 361, Series B, vol. 4 (1933); 1950. NACA TM 1292.
[6] Dipprey DF, Sabersky RH. Heat and momentum transfer in smooth and rough tubes at various Prandtl numbers. Int J Heat Mass Transf 1963;6:329–53.
[7] Webb RL, Eckort ERG, Goldstein KJ. Heat transfer and friction in tubes with repeated rib roughness. Int J Heat Mass Transf 1971;14:601–17.
[8] Firth RJ, Meyer L. A comparison of the heat transfer and friction factor performance of four different types of artificially roughened surface. Int J Heat Mass Transf 1983;26(2):175–83.
[9] Prasad BN, Saini JS. Effect of artificial roughness on heat transfer and friction factor in a solar air heater. Sol Energy 1988;6:555–60.
[10] Karwa Rajendra, Chauhan Kalpana. Performance evaluation of solar air heaters having V-down discrete rib roughness on the absorber plate. Energy 2010;35:398–409.
[11] Han JC, Glicksman LR, Rohsenow WM. An investigation of heat transfer and friction for rib roughened surfaces. Int J Heat Mass Transf 1978;21:1143–56.
[12] Taslim ME, Li T, Kerche DM. Experimental heat transfer and friction in channels roughened with angled, V-shaped and discrete ribs on two opposite walls. ASME J Turbomach 1996;118:20–8.
[13] Karwa R, Solanki SC, Saini JS. Heat transfer coefficient and friction factor correlations for the transitional flow regime in rib roughened rectangular ducts, vol. 42; 1999. p. 1597–1615.
[14] Han JC, Park JS. Developing heat transfer in rectangular channels with rib turbulators. Int J Heat Mass Transf 1988;31:183–95.
[15] Yeh Ho-Ming, Lin Chi-Yen. The effect of collector aspect ratio on the collector efficiency of upward-type flat-plate solar air heaters. Energy 1996;21:843–50.
[16] Wojciech M Budzianowski. Experimental and numerical study of recuperative heat recirculation. Heat Transf Eng 2012;33:712–21.
[17] Bhargava AK, Rizzi G. A solar air heater with variable flow passage width. Energy Convers Manag 1990;30:329–32.
[18] Verma R, Chandra R, Garg HP. Optimization of solar air heaters of different designs. Renew Energy 1992;2(521):531.
[19] Hegazy Adel A. Optimization of flow channel depth for conventional flat-plate solar air heaters. Renew Energy 1996;7:15–21.
[20] Hsieh Shou-shing, Shih Huei-Jan, Hong Ying-Jong. Laminar forced convection from surface-mounted ribs. Int J Heat Mass Transf 1990;33:1987–99.
[21] Hong Ying-Jong, Hseih Shou Shing. An experimental investigation of heat transfer characteristics for turbulent flow over staggered ribs in a square duct. Exp Therm Fluid Sci 1991;4:714–22.

[22] Hwang Jenn-Jiang, Liou Tong-Miin. Heat transfer and friction in a low-aspect-ratio rectangular channel with staggered slit-ribbed walls. Int J Rotat Mach 1998;4:283–91.
[23] Gao Xiufang, Sunden Bengt. Heat transfer and pressure drop in rib roughened rectangular duct. Exp Therm Fluid Sci 2001;24:25–34.
[24] Murata Akira, Mochizuki Sadanari. Comparison between laminar and turbulent heat transfer in a stationary square duct with transverse or angled rib turbulators. Int J Heat Mass Transf 2001;44:1127–41.
[25] Ahn SW. The effects of roughness types on friction factors and heat transfer in roughened rectangular duct. Int J Heat Mass Transf 2001;28:933–42.
[26] Chandra PR, Alexander CR, Han JC. Heat transfer and friction behaviors in rectangular channels with varying number of ribbed walls. Int J Heat Mass Transf 2003;46:481–95.
[27] Tanda Giovanni. Heat transfer in rectangular channels with transverse and V-shaped broken ribs. Int J Heat Mass Transf 2004;47:229–43.
[28] Tariq Andallib, Singh Kamlesh, Panigrahi PK. Detailed measurement of heat transfer and flow characteristics in rectangular duct with rib turbulators mounted on the bottom surface. Eng Turbul Model Exp 2002;5:445–54.
[29] Won SY, Ligrani PM. Comparisons of flow structure and local Nusselt numbers in channels with parallel- and crossed-rib turbulators. Int J Heat Mass Transf 2004;47:1573–86.
[30] Wang Lieke, Sunden Bengt. An experimental investigation of heat transfer and fluid flow in a rectangular duct with broken V-shaped ribs. Exp Heat Transf 2004;17:243–59.
[31] Liu Ye-Di, Diaz LA, Suryanarayana NV. Heat transfer enhancement in air heating fiat-plate solar collectors. Trans ASME J Sol Energy Eng 1984;106:358–63.
[32] Prasad K, Mullick SC. Heat transfer characteristics of a solar air heater used for drying purposes. Appl Energy 1983;13:83–93.
[33] Gupta D, Solanki SC, Saini JS. Heat and fluid flow in rectangular solar air heater ducts having transverse rib roughness on absorber plates. Sol Energy 1993;51:31–7.
[34] Saini RP, Saini JS. Heat transfer and friction factor correlations for artificially roughened ducts with expanded metal mesh as roughness element. Int J Heat Mass Transf 1995;40:973–86.
[35] Gupta Dhananjay, Solanki SC, Saini JS. Thermohydraulic performance of solar air heaters with roughened absorber plates, vol. 61; 1997. p. 33–42.
[36] Ekkad Srinath V, Han Je-chin. Detailed heat transfer distributions in two-pass square channels with rib turbulators. Int J Heat Mass Transf 1997;40:2525–37.
[37] Verma SK, Prasad BN. Investigation for the optimal thermo hydraulic performance of artificially roughened solar air heaters. Renew Energy 2000;20:19–36.
[38] Singh Sukhmeet, Chander Subhash, Saini JS. Heat transfer and friction factor correlations of solar air heater ducts artificially roughened with discrete V-down ribs. Energy 2011;36:5053–64.
[39] Ebrahim Momin Abdul-Malik, Saini JS, Solanki SC. Heat transfer and friction in solar air heater duct with V-shaped rib roughness on absorber plate.Int. Int J Heat Mass Transf 2002;45:3383–96.
[40] Karwa R. Experimental studies of augmented heat transfer and friction in asymmetrically heated rectangular ducts with ribs on the heated wall in transverse, inclined, V- continuous and V-discrete pattern. Int J Heat Mass Transf 2003;30:241–50.
[41] Sahu MM, Bhagoria JL. Augmentation of heat transfer coefficient by using 908 broken transverse ribs on absorber plate. Renew Energy 2005;30:2057–73.
[42] Jaurker AR, Saini JS, Gandhi BK. Heat transfer and friction characteristics of rectangular solar air heater duct using rib-grooved artificial roughness. Sol Energy 2006;80:895–907.
[43] Mittal MK, Varun, Saini RP, Singal SK. Effective efficiency of solar air heaters having different types of roughness elements on the absorber plate. Energy 2007;32:739–45.
[44] Karmare SV, Tikekar AN. Heat transfer and friction factor correlation for artificially roughened duct with metal grit ribs. Int J Heat Mass Transf 2007;50:4342–51.
[45] Aharwal KR, Gandhi BK, Saini JS. Experimental investigation on heat-transfer enhancement due to a gap in an inclined continuous rib arrangement in a rectangular duct of solar air heater. Renew Energy 2008;33:585–96.
[46] Saini RP. Verma Jitendra.Heat transfer and friction factor correlations for a duct having dimple-shape artificial roughness for solar air heaters. Energy 2008;3:1277–87.
[47] Saini SK, Saini RP. Development of correlations for Nusselt number and friction factor for solar air heater with roughened duct having arc-shaped wire as artificial roughness. Sol Energy 2008;82:1118–30.
[48] Layek Apurba, Saini JS, Solanki SC. Effect of chamfering on heat transfer and friction characteristics of solar air heater having absorber plate roughened with compound turbulators. Renew Energy 2009;34:1292–8.
[49] Kumar Arvind, Bhagoria JL, Sarviya RM. Heat transfer and friction correlations for artificially roughened solar air heater duct with discrete W-shaped ribs. Energy Convers Manag 2009;50:2106–17.
[50] Aharwal KR, Gandhi Bhupendra K, Saini JS. Heat transfer and friction characteristics of solar air heater ducts having integral inclined discrete ribs on absorber plate. Int J Heat Mass Transf 2009;52:5970–7.
[51] Gupta MK, Kaushik SC. Performance evaluation of solar air heater having expanded metal mesh as artificial roughness on absorber plate. Int J Therm Sci 2009;48:1007–16.
[52] Karmare SV, Tikekar AN. Experimental investigation of optimum thermohydraulic performance of solar air heaters with metal rib grits roughness. Sol Energy 2009;83:6–13.
[53] Bopche Santosh B, Tandale Madhukar S. Experimental investigations on heat transfer and frictional characteristics of a turbulator roughened solar air heater duct. Int J Heat Mass Transf 2009;52:2834–48.
[54] Patnaik Varun, Saini Amar, Singal RP, Siddhartha SK. Performance prediction of solar air heater having roughened duct provided with transverse and inclined ribs as artificial roughness. Renew Energy 2009;34:2914–22.
[55] Hans VS, Saini RP, Saini JS. Heat transfer and friction factor correlations for a solar air heater duct roughened artificially with multiple V-ribs. Sol Energy 2010;84:898–911.
[56] Lanjewar A, Bhagoria JL, Sarviya RM. Heat transfer and friction in solar air heater duct with W-shaped rib roughness on absorber plate. Energy 2011;36:4531–41.
[57] Tanda Giovanni. Performance of solar air heater ducts with different types of ribs on the absorber plate. Energy 2011;36:6651–60.
[58] Lanjewar A, Bhagoria JL, Sarviya RM. Experimental study of augmented heat transfer and friction in solar air heater with different orientations of W-Rib roughness. Exp Therm Fluid Sci 2011;35:986–95.
[59] Kumar Anil, Saini RP, Saini JS. Experimental investigation on heat transfer and fluid flow characteristics of air flow in a rectangular duct with multi v-shaped rib with gap roughness on the heated plate, vol. 86; 2012. p. 1733–49.
[60] Brij Bhushan, Ranjit Singh. Nusselt number and friction factor correlations for solar air heater duct having artificially roughened absorber plate. Sol Energy 2011;85:1109–18.
[61] Bhusan Brij, Singh Ranjit. Thermal and thermohydraulic performance of roughened solar air heater having protruded absorber plate. Sol Energy 2012;86:3388–96.
[62] Sethi Muneesh, Varun Thakur NS. Correlations for solar air heater duct with dimpled shape roughness elements on absorber plate. Sol Energy. 2012;86:2852–61.
[63] Singh Sukhmeet, Chander Subhash, Saini JS. Investigations on thermohydraulic performance due to flow-attack-angle in V-down rib with gap in a rectangular duct of solar air heater. Appl Energy 2012;97:907–12.
[64] Kumar Anil, Saini RP, Saini JS. Development of correlations for Nusselt number and friction factor for solar air heater with roughened duct having multi V-shaped with gap rib as artificial roughness. Renew Energy 2013;58:151–63.
[65] Prasad BN. Thermal performance of artificially roughened solar air heaters. Sol Energy 2013;9:159–67.
[66] Rajendra Karwa, Girish Chitoshiya. Performance study of solar air heater having V-down discrete ribs on absorber plate. Energy 2013;5:939–55.
[67] Sanjay Yadav, Maneesh Kaushal, Siddhartha Varun. Nusselt number and friction factor correlations for solar air heater duct having protrusions as roughness elements on absorber plate. Exp Therm Fluid Sci 2013;44:34–41.
[68] Mulluwork KB. Studies on discrete rib roughened solar air heaters. Proc NSEC 1998:75–84.
[69] Karwa R, Solanki, Solanki SC, Saini JS. Heat transfer coefficient and friction factor correlations for the transitional flow regime in rib roughened rectangular ducts. Int J Heat Mass Transf 1999;42:1597–615.
[70] Bhagoria JL, Saini JS, Solanki SC. Heat transfer coefficient and friction factor correlations for rectangular solar air heater duct having transverse wedge shaped rib roughness on the absorber plate. Renew Energy 2002;25:341–69.
[71] Gupta A, Harsha V, Prabhu V. Local heat transfer distribution in a square channel with 90° continuous, 90° saw tooth profiled and 60° broken ribs, vol. 32; 2008. p. 997–1010.
[72] Varun Saini RP, Singal SK. Investigation of thermal performance of solar air heater having roughness elements as a combination of inclined and transverse ribs on the absorber plate. Renew Energy 2008;33:1398–405.
[73] Singh Sukhmeet, Chander Subhash, Saini JS. Heat transfer and friction factor correlations of solar air heater ducts artificially roughened with discrete V-down ribs. Energy 2011;36:5053–64.
[74] Gill RS, Singh Sukhmeet, Singh Parm Pal. Energy Convers Manag 2012;57:131–42.
[75] Gupta D. Investigations on fluid flow and heat transfer in solar air heaters with roughened absorbers. (PhD. thesis). University of Roorkee; 1994.